# Analytical Approach for the Flexural Analysis of RC Beams Strengthened with Prestressed CFRP

Mohammadali Rezazadeh,[1] Joaquim Barros,[2] Inês Costa,[3]

**ABSTRACT**: The objective of this paper is to propose a simplified analytical approach to predict the flexural behavior of simply supported reinforced-concrete (RC) beams flexurally strengthened with prestressed carbon fiber reinforced polymer (CFRP) reinforcements using either externally bonded reinforcing (EBR) or near surface mounted (NSM) techniques. This design methodology also considers the ultimate flexural capacity of NSM CFRP strengthened beams when concrete cover delamination is the governing failure mode. A moment-curvature ( $M-\chi$ ) relationship formed by three linear branches corresponding to the precracking, postcracking, and postyielding stages is established by considering the four critical $M-\chi$ points that characterize the flexural behavior of CFRP strengthened beams. Two additional $M-\chi$ points, namely, concrete decompression and steel decompression, are also defined to assess the initial effects of the prestress force applied by the FRP reinforcement. The mid-span deflection of the beams is predicted based on the curvature approach, assuming a linear curvature variation between the critical points along the beam length. The good predictive performance of the analytical model is appraised by simulating the force-deflection response registered in experimental programs composed of RC beams strengthened with prestressed NSM CFRP reinforcements.

Keywords: Analytical approach, flexural analysis, RC beams, prestressed CFRP reinforcement, concrete cover delamination.

[1] ISISE, PhD student of the Structural Division of the Dep. of Civil Engineering, University of Minho, 4800-058 Guimarães, Portugal. rzh.moh@gmail.com
[2] ISISE, Full Professor of the Structural Division of the Dep. of Civil Engineering, University of Minho, 4800-058 Guimarães, Portugal. barros@civil.uminho.pt
[3] ISISE, PhD student of the Structural Division of the Dep. of Civil Engineering, University of Minho, 4800-058 Guimarães, Portugal. ines.costa@civitest.com

## 1. Introduction

Carbon fiber reinforced polymer (CFRP) systems have been extensively investigated for the flexural and shear strengthening of reinforced concrete (RC) structures due to their advantages, like high strength and stiffness to weight ratios, excellent fatigue behavior, and high durability in environment conditions where conventional materials have serious concerns in terms of degradation of their properties [1-3]. CFRP composite materials can be applied to RC structures to be strengthened by using either externally bonded reinforcing (EBR) or near surface mounted (NSM) techniques [4, 5]. Experimental research has demonstrated that NSM technique is more effective in shear and flexural strengthening than the EBR technique due to the higher ratio of the bond contact area to the cross sectional area, as well as the higher confinement to the CFRP provided by the surrounding concrete [6-9].

Nordin and Taljsten applied a prestress force to the NSM CFRP reinforcement for the flexural strengthening of RC beams resulting a better utilization of these high tensile strength materials [10]. In fact, applying an appropriate prestress level on the CFRP reinforcement can significantly increase the load carrying capacity corresponding to concrete cracking and steel yielding initiations, as well as an increase of the load at serviceability limit state (SLS) conditions [11-13]. Prestressed CFRPs can also decrease the deflection and crack width when compared to the corresponding results obtained with non-prestressed CFRPs [14, 15].

The possible flexural failure modes for the RC beams strengthened with CFRP reinforcement using EBR or NSM techniques can be classified into distinct categories, namely: tension failure of CFRP, concrete compression failure, delamination of concrete cover, and CFRP debonding [1, 16]. Although the ultimate flexural capacity of RC beams can be increased significantly by using CFRP reinforcement, its efficiency for the flexural strengthening may be limited by the occurrence of concrete cover delamination (rip-off) as a premature failure mode [15]. Concrete cover delamination can occur due to the formation and propagation of a fracture surface in the concrete cover at the free extremity of the CFRP reinforcement. Many studies have been carried out to identify the load carrying capacity of EBR CFRP strengthened RC beam failing by concrete cover delamination [17-19]. For the NSM technique, however, a formulation with physical and mechanical support for the prediction of this type of failure mode, with a format that can be used in a design context of RC beams flexurally strengthened with CFRP systems, still does not exist. Therefore, the present work has also the purpose of developing this type of formulation.

The moment-curvature relationship of the cross section of RC beams can be idealized as a trilinear diagram representing the uncracked, cracked, and yielded stages of a RC beam [20]. A trilinear moment-curvature response was considered by Saqan and Rasheed for rectangular cross section beams reinforced with prestressed steel strands in order to compute the neutral axis depth with a simple hand calculation instead of iterative numerical procedure for the cracked section [21]. On the other hand, the flexural capacity and the deformational behavior of CFRP strengthened beams can analytically be predicted by using a trilinear moment-curvature relationship based on the strain compatibility and principles of static equilibrium. El-Mihilmy and Tedesco, and Rasheed et al. adopted a trilinear relationship for the flexural response of RC beams flexurally strengthened with FRP plates [22, 23]. El-Mihilmy and Tedesco also proposed a method for calculating the deflection using the developed effective moment of inertia for FRP-strengthened RC beams, while Rasheed et al. determined the deflection by integrating the curvature along the beam length. The deflection of the strengthened beams can also be estimated based on the integration of the curvature in the uncraked and cracked sections representing a certain number of elements with the length equal to average crack spacing [11]. Barros and Dalfré proposed an analytical approach to calculate the deflection of RC structures strengthened according to NSM or EBR technique based on the force method, also known as flexibility method, consisting on establishing a set of displacement compatibility equations whose number is equal to the unknown redundant supports and generalized displacements (or forces) to be determined [24].

The current study intends to propose an analytical formulation, with a design framework, based on the strain compatibility and principles of static equilibrium to predict moment-curvature and force-deflection relationships of RC beams flexurally strengthened with prestressed CFRP reinforcement. The moment-curvature response of the prestressed section is simulated by the proposed simplified trilinear diagram (representing the precracking, postcracking, and postyielding stages) consisting two stages up to concrete crack initiation (precracking stage) in order to simulate the effect of the prestressing. One of these stages refers to concrete decompression, and the other to steel decompression. In fact, according to this analytical approach, the influence of the prestress force on the trilinear moment-curvature response of the non-prestressed section can be considered by adding the strain profile of the cross section at the concrete and steel decompression points to the corresponding strain values in the non-prestressed section at the concrete cracking and steel yielding initiation points, respectively. Furthermore, the analytical equations are proposed to determine the neutral axis depth of the cracked non-prestressed and prestressed strengthened sections at the critical points in order to provide a simple hand calculation and eliminate the iterative numerical procedure. The

developed design methodology also considers the possibility of occurring the concrete cover delamination failure mode, since this can limit the ultimate flexural load carrying capacity of RC beams strengthened with NSM CFRP reinforcement. This methodology is developed by considering the influence of the effective parameters on the occurrence of the concrete cover delamination failure mode.

The force versus mid-span deflection of the beam is analytically predicted using the curvature distribution along the beam length. The calculation complexities are simplified by assuming a linear curvature variation between the critical points that decompose the beam in the three regions corresponding to the trilinear flexural behavior.

The developed analytical formulation can be also applied on the design of RC slabs strengthened with FRP systems other than CFRP reinforcements. The predictive performance of the analytical model is assessed by simulating the tests of experimental studies, consisting of RC beams flexurally strengthened with prestressed or non-prestressed NSM CFRP reinforcements.

## 2. Assumptions

The following assumptions were adopted in the proposed analytical model:

a) Strain in the longitudinal steel bars, CFRP reinforcement and concrete is directly proportional to their distance from the neutral axis of the cross section of the RC element;
b) There is no slip between steel and CFRP reinforcements and surrounding concrete when conventional flexural failure modes are considered as the prevailing ones;
c) The maximum compressive strain in concrete is 0.003.

## 3. Analytical Approach

As already mentioned, the moment-curvature ( $M-\chi$ ) relationship of the cross section of a prestressed strengthened RC beam can be idealized by a trilinear diagram representing the precracking, postcracking, and postyielding phases, delimited by the following $M-\chi$ points (Figure 1): initial camber (point (ci)); concrete crack initiation (point (cr));

steel yield initiation (point (y)); and ultimate capacity (point (u)). The strain distribution on the beam cross section at each of these points is also schematically represented in Figure 1.

When releasing the prestress force an initial compression field in the longitudinal steel bars and surrounding concrete is introduced [11, 13]. By applying an increasing external load, these compressive strains are converted in tensile strains. The transition from compressive to tensile strain (null strain) at the bottom fiber of concrete and at the longitudinal steel bars is defined as the concrete decompression point (point (cd) in Figure 1) and steel decompression point (point (sd) in Figure 1), respectively. As expected, the load carrying capacity corresponding to the concrete cracking and steel yielding initiation increase with the level of prestress due to this initial compressive strain profile. Hence, the strain profile of the cross section at the concrete decompression and steel decompression instants should be added to the corresponding strain values in the non-prestressed strengthened beam at the concrete cracking and steel yielding initiation points, respectively, as represented in Figure 2 (see sections 5.1 and 5.2). It should be mentioned that both decompression points do not exist when non-prestressed FRP reinforcement is applied.

The analytical model detects the ultimate flexural capacity of the strengthened beams adopting three types of failure modes, namely: concrete crushing, tensile rupture of the CFRP, and concrete cover delamination. Firstly, the possibility of occurring either concrete crushing or tensile rupture of the CFRP (conventionally known as flexural failure modes) is evaluated by considering a critical percentage of CFRP reinforcement ( $\rho_f^{(cri)}$ ) that assures the simultaneous occurrence of the aforementioned failures. A CFRP reinforcement ratio higher than this critical percentage causes a concrete crushing failure mode, otherwise the tensile rupture of the CFRP reinforcement is the dominant failure mode (see section 5.3.1). In the next stage, the ultimate flexural capacity of the strengthened beam when failing by concrete cover delamination is determined. Finally, the ultimate flexural capacity governed by conventional flexural failure modes is compared to the one conditioned by the concrete cover delamination, in order to determine the prevailing failure mode (see section 5.3.2).

Figure 3 schematically represents the geometry and reinforcement details of the simply supported strengthened beam adopted for the analytical study. The beam is assumed to be subjected to a four-point loading configuration. The analytical approach can be also applied in case of monotonic three-point bending loading by considering a null loading span ( $a_L = 0$ ). A more detailed description of the analytical model reported in this paper can be found elsewhere [25].

## 4. Constitutive Law of the Materials

The compressive behavior of concrete is assumed linear up to the yielding of the longitudinal steel reinforcement in order to simplify the calculation procedure. After steel yielding, the contribution of concrete in compression is simulated by a rectangular compressive stress block, defined by the $\alpha_1$ and $\beta_1$ parameters (Eq. (1)) schematically represented in Figure 4a [1].

$$\beta_1 = \frac{4.\varepsilon_c^{'} - \varepsilon_c}{6.\varepsilon_c^{'} - 2.\varepsilon_c} \quad (1)\text{-a}$$

$$\alpha_1 = \frac{3.\varepsilon_c^{'}.\varepsilon_c - \varepsilon_c^{\,2}}{3.\beta_1.\varepsilon_c^{'\,2}} \quad (1)\text{-b}$$

where $\varepsilon_c^{'}$ is the strain corresponding to the specified compressive strength of concrete $f_c^{'}$, which is calculated as:

$$\varepsilon_c^{'} = \frac{1.7 f_c^{'}}{E_c} \quad (2)$$

The tensile behavior of concrete is assumed linear up to the stress at concrete crack initiation in concrete tensile surface [26]. An elasto-perfectly plastic model is used to simulate the behavior of the longitudinal steel bars, as represented in Figure 4b, while a linear behavior is adopted for the CFRP up to its ultimate tensile strength (Figure 4c).

## 5. Moment-Curvature Relationship

The analytical approach defines the moment-curvature response of the cross section of a RC element flexurally strengthened with CFRP reinforcements (failing in bending) using sectional analysis based on the strain compatibility and force equilibrium at the governing stages assumed representatives of the behavior of this type of elements.

### *5.1. Precracking Stage*

When the CFRP reinforcement is applied with a certain prestress level, an initial negative camber (upward deflection) is obtained due to the eccentricity ( $e$ ) of the prestress force ( $F_{pre}$ ) in relation to the centroidal axis of the cross section ( $y_i$ , Figure 4a) at the precracking stage. This negative camber causes a tensile strain at the top fiber ( $\varepsilon_{cc}^{(ci)}$ ) and a compressive strain at the bottom fiber ( $\varepsilon_{ct}^{(ci)}$ ) of concrete, whose equations are provided in Appendix A1.

The initial negative curvature of the prestressed strengthened beams ( $\chi^{(ci)}$ ) can be determined by considering the neutral axis depth from the extreme top fiber of concrete ( $c^{(ci)}$ ) as follows:

$$c^{(ci)} = \frac{\varepsilon_{cc}^{(ci)}.h}{\left(\varepsilon_{cc}^{(ci)} + \varepsilon_{ct}^{(ci)}\right)} \rightarrow \chi^{(ci)} = \frac{\varepsilon_{cc}^{(ci)}}{c^{(ci)}} \tag{3}$$

A loss of strain in the CFRP reinforcement occurs immediately after the total release of the prestress force due to the initial negative camber. This short-term prestrain loss ( $\varepsilon_{lf}^{(ci)}$ ) and effective tensile strain ( $\varepsilon_{ef}^{(ci)}$ ) in the CFRP reinforcement are determined from the following equations:

$$\varepsilon_{lf}^{(ci)} = \frac{\varepsilon_{cc}^{(ci)}.\left(d_f - c^{(ci)}\right)}{c^{(ci)}} \rightarrow \varepsilon_{ef}^{(ci)} = \varepsilon_{fp} - \varepsilon_{lf}^{(ci)} \tag{4}$$

where $d_f$ is the internal arm of the CFRP (Figures 3b and 3c) and $\varepsilon_{fp}$ is the applied prestrain.

The concrete decompression point ((cd) in Figure 1) corresponds to the stage where the initial compressive strain in the bottom fiber of concrete ( $\varepsilon_{ct}^{(ci)}$ ) becomes zero, resulting in a neutral axis depth equal to $h$, while the steel decompression point ((sd) in Figure 1) refers to the stage when the initial compressive strain in the bottom longitudinal steel bars ( $\varepsilon_s^{(ci)}$ ), due to prestress application, becomes null, at which $d_s$ is the neutral axis depth. The curvature at concrete decompression ( $\chi^{(cd)}$ ) and steel decompression ( $\chi^{(sd)}$ ) points can be assessed by adopting the ratio between the compressive strain installed on the concrete top fiber ( $\varepsilon_{cc}$ ) at each point (Eq. (5)) and the corresponding neutral axis depth [25]. Strains in the constituent materials along the depth of the cross section (longitudinal top ( $\varepsilon_s^{'}$ ) and bottom ( $\varepsilon_s$ ) steel bars, and in the CFRP reinforcement ( $\varepsilon_f$ )) are directly proportional to the distance from the neutral

axis depth at each decompression point, while the concept of effective tensile strain should be adopted for the prestressed CFRP reinforcement (see Appendix A2 and Figure 2).

$$\varepsilon_{cc}^{(cd)} = \varepsilon_{cc}^{(ci)} - \frac{\left|\varepsilon_{ct}^{(ci)}\right|.y_i}{\left(h - y_i\right)} \quad (5)\text{-a}$$

$$\varepsilon_{cc}^{(sd)} = \varepsilon_{cc}^{(ci)} - \frac{\left|\varepsilon_{s}^{(ci)}\right|.y_i}{\left(d_s - y_i\right)} \quad (5)\text{-b}$$

The flexural bending moment at the concrete decompression ( $M^{(cd)}$ ) and steel decompression ( $M^{(sd)}$ ) points can be derived based on the sum of internal moments with respect to the corresponding neutral axis using the strain distribution of the section [25]:

$$M^{(cd)} = \frac{1}{3}\varepsilon_{cc}^{(cd)}.b.E_c.h^2 + \varepsilon_s^{'(cd)}.E_s.A_s^{'}.\left(h - d_s^{'}\right) + \varepsilon_s^{(cd)}.E_s.A_s.\left(h - d_s\right) + \varepsilon_{ef}^{(cd)}.E_f.A_f.\left(d_f - h\right) \quad (6)$$

$$M^{(sd)} = \frac{1}{3}\varepsilon_{cc}^{(sd)}.b.E_c.d_s^2 + \varepsilon_s^{'(sd)}.E_s.A_s^{'}.\left(d_s - d_s^{'}\right) + \frac{1}{3}\varepsilon_{ct}^{(sd)}.b.E_c.\left(h - d_s\right)^2 + \varepsilon_{ef}^{(sd)}.E_f.A_f.\left(d_f - d_s\right) \quad (7)$$

The steel decompression point is followed by the concrete crack initiation, where the beam still exhibits linear elastic behavior, but the tensile strain at the extreme bottom fiber of concrete ( $\varepsilon_{ctb}^{(cr)}$ ) reaches its flexural tensile strength ( $\varepsilon_{ct} = f_r / E_c \rightarrow f_r = 0.62\sqrt{f_c^{'}}$ [26]) (Figure 2a). The strains in the constituent materials along the cross section are proportional to the distance from the centroidal axis of the beam cross section ( $y_i$ ) (Figure 2a). The increment of curvature and flexural capacity corresponding to the bending moment between the concrete decompression and crack initiation points can be obtained from Eqs. (8) and (9) in relation to the centroidal axis of the beam cross section ( $y_i$ ).

$$\chi_b^{(cr)} = \frac{\varepsilon_{ccb}^{(cr)}}{y_i} \quad (8)$$

$$M_b^{(cr)} = \frac{1}{3}\varepsilon_{ccb}^{(cr)}.b.E_c.y_i^2 + \varepsilon_{sb}^{'(cr)}.E_s.A_s^{'}.\left(y_i - d_s^{'}\right) + \frac{1}{3}\varepsilon_{ctb}^{(cr)}.b.E_c.\left(h - y_i\right)^2 + \varepsilon_{sb}^{(cr)}.E_s.A_s.\left(d_s - y_i\right) + \varepsilon_{fb}^{(cr)}.E_f.A_f.\left(d_f - y_i\right) \quad (9)$$

where the equations for the determination of the strain components are provided in Appendix A3. Finally, the curvature ( $\chi^{(cr)}$ ) and flexural bending moment ( $M^{(cr)}$ ) of the prestressed strengthened beams at the concrete crack initiation can be determined by using Eqs. (10) and (11), where the $\chi^{(cd)}$ and $M^{(cd)}$ are considered null for the non-prestressed beam (Figure 2a).

$$\chi^{(cr)} = \chi^{(cd)} + \chi_b^{(cr)} \tag{10}$$

$$M^{(cr)} = M^{(cd)} + M_b^{(cr)} \tag{11}$$

### *5.2. Postcracking Stage*

The steel yield initiation point corresponds to the stage where the strain in the longitudinal tensile steel reinforcement ( $\varepsilon_{sb}^{(y)}$ ) reaches its yield strength ( $\varepsilon_{sy} = f_{sy}/E_s$ ). The steel decompression point should be introduced as an initial condition for the steel yield initiation instant. Accordingly, to determine the strain distribution of the cross section at the steel yield initiation point, the strain profile of the cross section at the steel decompression instant should be added to the corresponding strain values of the cross section due to the bending moment after this decompression point (Figure 2b).

The strain profile of the cross section due to the bending moment between the steel decompression and steel yield initiation points can be obtained adopting the proportional strain distribution to the distance from the neutral axis depth ( $c_b^{(y)}$ ) by considering the strain value in the longitudinal tensile steel bars ( $\varepsilon_{sb}^{(y)}$ ) [25]. According to the principles of static equilibrium, a quadratic equation is obtained to calculate the neutral axis depth ( $c_b^{(y)}$ ) at the steel yield initiation stage due to the bending moment after the steel decompression point (Eq. (12)) (see Appendix A4).

$$a.c_b^{(y)2} + b.c_b^{(y)} + c = 0 \tag{12}\text{-a}$$

where

$$a = E_c.b$$
$$b = 2.\left(E_s.A_s^{'} + E_s.A_s + E_f.A_f\right) \quad \text{(12)-b}$$
$$c = -2.\left(E_s.A_s^{'}.d_s^{'} + E_s.A_s.d_s + E_f.A_f.d_f\right)$$

The increment of curvature ( $\chi_b^{(y)}$ ) and flexural capacity ( $M_b^{(y)}$ ) corresponding to the bending moment between the steel decompression and yield initiation points can be determined by Eqs. (13) and (14), respectively, with regard to the neutral axis depth ( $c_b^{(y)}$ ).

$$\chi_b^{(y)} = \frac{\varepsilon_{ccb}^{(y)}}{c_b^{(y)}} \quad (13)$$

$$M_b^{(y)} = \frac{1}{3}\varepsilon_{ccb}^{(y)}.E_c.b.c_b^{(y)2} + \varepsilon_{sb}^{'(y)}.E_s.A_s^{'}.\left(c_b^{(y)} - d_s^{'}\right) + \varepsilon_{sb}^{(y)}.E_s.A_s.\left(d_s - c_b^{(y)}\right) + \varepsilon_{fb}^{(y)}.E_f.A_f.\left(d_f - c_b^{(y)}\right) \quad (14)$$

Finally, the curvature ( $\chi^{(y)}$ ) and flexural bending moment ( $M^{(y)}$ ) of the prestressed strengthened beams at the steel yield initiation point are determined using Eqs. (15) to (16), where the $\chi^{(sd)}$ and $M^{(sd)}$ are considered null for the non-prestressed strengthened beam (Figure 2b).

$$\chi^{(y)} = \chi^{(sd)} + \chi_b^{(y)} \quad (15)$$

$$M^{(y)} = M^{(sd)} + M_b^{(y)} \quad (16)$$

### *5.3. Postyielding Stage*

The ultimate flexural capacity of the strengthened beams is controlled by adopting three types of failure modes, namely, yielding of the steel bars in tension followed by either concrete crushing or rupture of the CFRP reinforcement (known as conventional flexural failure modes), and delamination of the concrete cover.

#### *5.3.1. Conventional flexural failure modes*

The concrete crushing is assumed to occur when the compressive strain on the concrete top fiber of the cross section reaches its maximum usable strain ( $\varepsilon_{cu} = 0.003$ according to the ACI-440.2R [1]), while the strengthened beams is

assumed to experience the rupture of the CFRP reinforcement when the ultimate tensile strain in the CFRP is achieved ($\varepsilon_{fu}$).

To assess the prevailing failure mode in the strengthened beams at the ultimate stage, a critical percentage of CFRP reinforcement ($\rho_f^{(cri)}$) can be determined assuming simultaneous tension and compression failures to detect the appropriate failure mode (Appendix A5). If the CFRP ratio exceeds the critical value, failure will be due to the concrete crushing, otherwise failure will be caused by rupture of the CFRP reinforcement. The critical area ($A_f^{(cri)}$) and the corresponding percentage ($\rho_f^{(cri)}$) for the CFRP reinforcement can be determined from:

$$A_f^{(cri)} = \frac{\alpha_1.f_c^{'}.\beta_1.c^{(cri)}.b + A_s^{'}.\varepsilon_s^{'(cri)}.E_s - A_s.f_{sy}}{\varepsilon_{fu}.E_f} \rightarrow \rho_f^{(cri)} = \frac{A_f^{(cri)}}{b.d_f} \tag{17}$$

*Concrete Crushing*

Concrete crushing will prevail at ultimate stage when the CFRP ratio exceeds the critical percentage. From the equilibrium of the internal forces results a quadratic equation that determines the neutral axis depth ($c_{cc}^{(u)}$) at failure (Appendix A5):

$$a.c_{cc}^{(u)\,2} + b.c_{cc}^{(u)} + c = 0 \tag{18-a}$$

where

$$\begin{aligned} a &= f_c^{'}.b.\left(3.\varepsilon_c^{'}.\varepsilon_{cu} - \varepsilon_{cu}^2\right) \\ b &= 3.\varepsilon_c^{'2}.\left(\varepsilon_{cu}.\left(E_s.A_s^{'} + E_f.A_f\right) - A_s.f_{sy} - E_f.A_f.\varepsilon_{fp}\right) \\ c &= -3.\varepsilon_c^{'2}.\varepsilon_{cu}.\left(E_s.A_s^{'}.d_s^{'} + E_f.A_f.d_f\right) \end{aligned} \tag{18-b}$$

The curvature ($\chi_{cc}^{(u)}$) and ultimate flexural capacity ($M_{cc}^{(u)}$) are obtained from the following equations (Appendix A5):

$$\chi_{cc}^{(u)} = \frac{\varepsilon_{cu}}{c_{cc}^{(u)}} \tag{19}$$

$$M_{cc}^{(u)} = \alpha_1.f_c^{'}.\beta_1.c_{cc}^{(u)\,2}.b.\left(1-\frac{\beta_1}{2}\right)+\varepsilon_{s,cc}^{'(u)}.E_s.A_s^{'}.\left(c_{cc}^{(u)}-d_s^{'}\right)+f_{sy}.A_s.\left(d_s-c_{cc}^{(u)}\right)+E_f.\varepsilon_{f,cc}^{(u)}.A_f.\left(d_f-c_{cc}^{(u)}\right) \quad (20)$$

*Rupture of CFRP Reinforcement*

The equilibrium of the internal forces at the cross section, when the rupture of the CFRP reinforcement occurs, can be derived adopting strain compatibility, resulting in a cubic equation, whose solution leads the depth of the neutral axis at ultimate stage ( $c_{rc}^{(u)}$ ) (Appendix A5):

$$a.c_{rc}^{(u)\,3}+b.c_{rc}^{(u)\,2}+c.c_{rc}^{(u)}+d=0 \quad (21)\text{-a}$$

where

$$\begin{aligned} a &= \varepsilon_{fb,rc}^{(u)}.f_c^{'}.b.\left(3.\varepsilon_c^{'}+\varepsilon_{fb,rc}^{(u)}\right)\\ b &= 3.\varepsilon_c^{'}.\left(\varepsilon_{fb,rc}^{(u)}.(\varepsilon_c^{'}.E_s.A_s^{'}-f_c^{'}.b.d_f)+\varepsilon_c^{'}.\left(A_f.f_{fu}+A_s.f_{sy}\right)\right)\\ c &= -3.\varepsilon_c^{'2}.\left(\varepsilon_{fb,rc}^{(u)}.E_s.A_s^{'}.\left(d_f+d_s^{'}\right)+2.d_f.\left(A_f.f_{fu}+A_s.f_{sy}\right)\right)\\ d &= 3.\varepsilon_c^{'2}.d_f.\left(\varepsilon_{fb,rc}^{(u)}.E_s.A_s^{'}.d_s^{'}+d_f.\left(A_f.f_{fu}+A_s.f_{sy}\right)\right) \end{aligned} \quad (21)\text{-b}$$

Accordingly, the curvature ( $\chi_{rc}^{(u)}$ ) and ultimate flexural capacity ( $M_{rc}^{(u)}$ ) regarding the neutral axis depth level ( $c_{rc}^{(u)}$ ) at CFRP failure is determined as follows (Appendix A5):

$$\chi_{rc}^{(u)}=\frac{\varepsilon_{cc,rc}^{(u)}}{c_{rc}^{(u)}} \quad (22)$$

$$M_{rc}^{(u)} = \alpha_1.f_c^{'}.\beta_1.c_{rc}^{(u)\,2}.b.\left(1-\frac{\beta_1}{2}\right)+\varepsilon_{s,rc}^{'(u)}.E_s.A_s^{'}.\left(c_{rc}^{(u)}-d_s^{'}\right)+f_{sy}.A_s.\left(d_s-c_{rc}^{(u)}\right)+f_{fu}.A_f.\left(d_f-c_{rc}^{(u)}\right) \quad (23)$$

5.3.2. Concrete cover delamination

Concrete cover delamination, also designated by rip-off, is initiated by forming an in-plane shear crack at the extremities of the CFRP reinforcement due to high strain gradient caused by the abrupt termination of the CFRP. This crack is propagated along the depth of the concrete cover of the beam up to attain the tensile steel reinforcement level, and then progresses horizontally along this level due to the resistance offered by this reinforcement to the propagation of the crack through it, as well as the higher percentage of voids just below this reinforcement [15, 18]. Subsequently,

separation of the concrete cover along the longitudinal tensile steel bars occurs in the shear span of the beam, which can compromise the flexural strengthening effectiveness of this technique if it occurs prematurely. Furthermore, the susceptibility to the concrete cover delamination in the NSM CFRP strengthened beams is influenced by some variables, such as the concrete strength class, reinforcement ratio of existing longitudinal steel bars, number and diameter of the bars composing this reinforcement, the relative position between the longitudinal steel and CFRP reinforcements, number of CFRP reinforcements, and distance between the consecutive CFRPs [27].

The present section aims to propose a new methodology to predict the ultimate flexural capacity of a RC beam strengthened with NSM CFRP laminates failing by concrete cover delamination. For this purpose, the concrete cover delamination is assumed to occur when the principal tensile stress transferred to the surrounding concrete at the extremity of the longitudinal CFRP laminate attains the concrete tensile strength ( $f_{ct} = 0.56\sqrt{f_c'}$ [26]). The present approach, for the tensile fracture surface of this surrounding concrete, was inspired on the work of Bianco et al. (2014) that proposed a semi-pyramidal shape for modeling the concrete resisting contribution during the pullout process of NSM FRP reinforcement bridging a shear failure crack in the context of the use of these composite materials and technique for the shear strengthening of RC beams [28]. Hence, in the current analytical model, the semi-pyramidal configuration was adopted for the concrete tensile fracture surface at the extremities of each CFRP laminate applied for flexural strengthening, as represented in Figure 5a.

The dimensions of this tensile fracture surface of the surrounding concrete (assumed by simplification as having a semi-pyramid format) are supposed to be limited by some restrictions to consider the influence of the aforementioned variables on the susceptibility of concrete cover delamination, and also simplify the model. These restrictions of the semi-pyramid on the beam's tensile surface aim to avoid interaction between the concrete fracture surfaces of consecutive CFRP laminates. On the other hand, due to the possibility of occurring a weak plan just beneath the tensile steel bars, the thickness of the semi-pyramid is limited to the concrete cover thickness ( $c_c$ ) (Figure 5c).

Accordingly, the semi-pyramidal concrete fracture surface is assumed to be extended until the base area of the semi-pyramid (rectangular shape) reaches a boundary limit. This boundary limit is defined when the short side of the rectangular base achieves the length of $c_c$ (Figure 5c), while the long side of this rectangular should be limited to $\min(s_f; 2s_f')$ for the CFRP laminates near the beam edge (side-laminates) and $s_f$ for the mid-laminates (Figure 5b).

However, considering that $s_f$ is in general higher than 40 mm (Barros and Kotynia 2008) and the angle $\alpha$ formed by the principal generatrices of the semi-pyramid with the CFRP longitudinal axis (Figures 5b and 5c) is presumed to be in the interval of 10 to 35 degrees (Bianco et al. 2014), the above boundary limit on the beam's tensile surface seems to be experimentally supported.

According to the base area and $\alpha$ of the semi-pyramid of the concrete fracture surface (Figures 5a and 5c), the height of the semi-pyramid can be defined as the resisting bond length ( $L_{rb}$ ), where the slip between the CFRP laminate and surrounding concrete is neglected along this length to calculate the resistance of the concrete fracture surface. The resistance of the concrete fracture surface for each CFRP laminate ( $F_{cf}$ ) can be determined by considering the concrete tensile strength ( $f_{ct}$ ). Accordingly, the ultimate flexural capacity of a strengthened beam developing a concrete cover delamination failure mode ( $M_{ccd}^{(u)}$ ) can be determined using the maximum applicable force to all the CFRP laminates at the end section of $L_{rb}$ (section A-A in Figures 5b and 5c).

The implementation of the proposed methodology to predict the concrete cover delamination as prevailing failure mode comprises the following steps (Figure 6): 1) providing the input parameters; 2) determination of the resisting bond length ( $L_{rb}$ ); 3) evaluation of the tensile strength of CFRP ( $F_{fu}$ ), maximum value of the force transferable through the resisting bond length ( $F_{rb}$ ), and concrete tensile fracture capacity ( $F_{cf}$ ) for each CFRP laminate; 4) assessment the possibility of the concrete tensile fracture at the end of the CFRP laminate considering the characteristics of bond conditions and the CFRP tensile strength; 5) determination of ultimate flexural capacity of the strengthened beam adopting concrete cover delamination failure; 6) evaluation the possibility of occurrence of the concrete cover delamination in comparison to the conventional prevailing failure modes including concrete crushing and rupture of the CFRP far from its extremities.

1) Input parameter

The input parameters include: concrete cover thickness $c_c$, angle $\alpha$ between principal generatrices of the semi-pyramidal fracture surface and the CFRP longitudinal axis, number of the longitudinal CFRP laminates $N$, distance

between two adjacent CFRP laminates $s_f$, distance between the beam edge and the nearest CFRP laminate $s_f^{'}$, thickness $a_f$ and width $b_f$ of laminate's cross section, and values of local bond stress-slip relationship: maximum shear stress $\tau_{\max}$ and maximum slip $\delta_{\max}$ (Figure 5).

2) Resisting bond length $L_{rb}$

The resisting bond length ( $L_{rb}$ ) at each extremity of the CFRP laminate can be calculated as follows:

$$L_{rb} = \frac{c_c}{\tan\alpha} \tag{24}$$

3) Tensile strength of CFRP $F_{fu}$, concrete tensile fracture capacity $F_{cf}$, and resisting bond force $F_{rb}$

Tensile strength of the CFRP laminate can be determined by Eq. (25). It should be noted that in the case of a round CFRP bar, its cross section is converted to an equivalent square cross sectional area.

$$F_{fu} = a_f . b_f . f_{fu} \tag{25}$$

The concrete tensile fracture capacity ( $F_{cf}$ ) of each CFRP laminate, adopting a semi-pyramidal fracture surface, can be determined considering the tensile resistance of concrete on the slant area of the semi-pyramid. It was evidenced that the concrete tensile resistance of the slant area is equivalent to simply multiplying the base area of semi-pyramid times the concrete tensile strength (Bianco 2008 [29]). Hence, for the current study, Eq. (26) is proposed to determine the concrete tensile fracture capacity ( $F_{cf}$ ) corresponding to each CFRP laminate.

$$F_{cf} = \min\left(2.L_{rb}.\tan\alpha \; ; \; 2.s_f^{'} \; ; \; s_f\right).c_c.f_{ct} \tag{26}$$

The maximum value of the force ( $F_{rb}$ ) that can be transferable through the resisting bond length ( $L_{rb}$ ) by the CFRP laminate can be obtained by Eq. (27) adopting an idealized local bond-slip relationship with a single softening branch as shown in Figure 5d (Bianco et al. 2014).

$$F_{rb}(L_{rb}) = L_p . \frac{1}{J_1} . \lambda . \left\{ C_1 . \left[ \cos\left(\lambda . L_{rb}\right) - 1 \right] - C_2 . \sin\left(\lambda . L_{rb}\right) \right\} \tag{27}\text{-a}$$

where

$$L_p = 2.b_f + a_f \;;\; J_1 = \frac{L_p}{\left(a_f.b_f\right)}.\left(\frac{1}{E_f} + \frac{\left(a_f.b_f\right)}{\left(A_c.E_c\right)}\right)$$
$$\frac{1}{\lambda^2} = \frac{\delta_{\max}}{\left(\tau_{\max}.J_1\right)} \;;\; C_1 = \delta_{\max} - \frac{\left(\tau_{\max}.J_1\right)}{\lambda^2} \;;\; C_2 = -\frac{\left(\tau_{\max}.J_1\right)}{\lambda^2} \quad (27)\text{-b}$$

and $A_c$ is the cross sectional area of the surrounding concrete that provides confinement to each CFRP laminate, and for side-laminates and mid-laminates can be obtained by Eqs. ((27)-c) and ((27)-d), respectively.

$$A_c = \min\left(2.s_f^{'}; s_f\right).c_c \quad (27)\text{-c}$$

$$A_c = s_f.c_c \quad (27)\text{-d}$$

The maximum bond force ( $F_{rb}$ ) for the resisting bond length ( $L_{rb}$ ) should be limited to the maximum debonding resistance ( $F_{rbe}$ ) and its corresponding effective resisting bond length ( $L_{rbe}$ ) given in Eq. (28) (Bianco et al. 2014).

$$L_{rbe} = \frac{\pi}{\left(2.\lambda\right)} \;;\; F_{rbe} = \frac{\left(L_p.\lambda.\delta_{\max}\right)}{J_1} \quad (28)$$

4) Assessment the possibility of concrete tensile fracture

This step of the algorithm aims to check which of the three types of failure modes occurs, namely, rupture of the CFRP, interfacial debonding failure, or concrete tensile fracture when the tensile force is applied to the CFRP laminate at the end section of resisting bond length (section A-A in Figure 5). In fact, the concrete tensile fracture can occur when the concrete tensile fracture capacity ( $F_{cf}$ ) corresponding to the CFRP laminate is a lower than the minimum of the tensile strength of the CFRP ( $F_{fu}$ ) and the resisting bond force ( $F_{rb}$ ). Otherwise, by increasing the applied force to the CFRP laminate at the section A-A represented in Figure 5, either the rupture of the CFRP or interfacial debonding failure would occur before the concrete tensile fracture (Figure 6).

5) Ultimate flexural capacity of the strengthened beam failed by concrete cover delamination

The effective concrete tensile fracture capacity ( $F_{cfe}$ ) of the CFRP laminates can be determined by summing the concrete tensile fracture capacity ( $F_{cf}$ ) of all the CFRP laminates flexurally applied on the tensile face of the beam (Eq. 29).

$$F_{cfe} = \sum_{i=1}^{N} F_{cfi} \tag{29}$$

The flexural capacity ( $M_{ccd}^{(Lrb)}$ ) of the strengthened beam at the end section of resisting bond length (section A-A in Figure 5) can be obtained by Eq. (30) using the effective concrete tensile fracture capacity ( $F_{cfe}$ ) of the CFRP laminates, where the beam's cross section is supposed to be located between the concrete cracking and steel yield initiation phases (postcracking stage). Otherwise, for the section located in the postyielding stage, the contribution of concrete in compression should be simulated by a rectangular compressive stress block (Eq. (1)), and the compressive and tensile strains in the longitudinal top and bottom steel bars, respectively, should be limited by its yield strength ( $\varepsilon_{sy} = f_{sy} / E_s$ ).

$$M_{ccd}^{(Lrb)} = \frac{1}{3}\varepsilon_{cc,ccd}.E_c.b.c_{ccd}^2 + \varepsilon_{s,ccd}^{'}.E_s.A_s^{'}.\left(c_{(ccd)} - d_s^{'}\right) + \varepsilon_{s,ccd}.E_s.A_s.\left(d_s - c_{ccd}\right) + F_{cfe}.\left(d_f - c_{ccd}\right) \tag{30}$$

where the strains of the components along the cross section can be determined adopting the proportional strain distribution to the distance from the neutral axis depth ( $c_{ccd}$ ) by considering the average tensile strain in the CFRP laminates ( $\varepsilon_{f,ccd} = F_{cfe} / (N.a_f.b_f.E_f)$ ).

According to the principles of static equilibrium and proportionality of the strain distribution along the cross section, the neutral axis depth ( $c_{ccd}$ ) can be obtained using a quadratic equation represented in Eq. (31).

$$a.{c_{ccd}}^2 + b.c_{ccd} + c = 0 \tag{31}\text{-a}$$

where

$$a = E_c.b$$
$$b = 2.\left(E_s.A_s^{'} + E_s.A_s + E_f.N.a_f.b_f\right) \quad (31)\text{-b}$$
$$c = -2.\left(E_s.A_s^{'}.d_s^{'} + E_s.A_s.d_s + E_f.N.a_f.b_f.d_f\right)$$

As a final point, the ultimate flexural capacity ($M_{ccd}^{(u)}$) of the NSM CFRP strengthened beam adopting the concrete cover delamination as prevailing failure mode is determined by Eq. (32) according to the bending moment distribution along the beam length (Figure 5a).

$$M_{ccd}^{(u)} = \frac{b_s.M_{ccd}^{(Lrb)}}{(L_{rb} + L_{ub})} \quad (32)$$

where $b_s$ is the distance between the support and the point load (shear span) and $L_{ub}$ is the unbonded length of the CFRP at each extremity of the laminate (shown in Figure 5).

6) Prevailing failure mode of the NSM CFRP strengthened beam

Occurrence of the concrete cover delamination of the strengthened beam can be expected when the corresponding ultimate flexural capacity ($M_{ccd}^{(u)}$) is lower than the ultimate flexural capacity of the prevailing conventional flexural failure mode obtained from section 5.3.1 ($M_{ccd}^{(u)} \le \min(M_{cc}^{(u)}; M_{rc}^{(u)})$) (Figure 6). On the other hand, the concrete cover delamination failure can occur after yielding of the longitudinal tensile steel bars when $M_{ccd}^{(u)}$ is higher than the flexural capacity of the beam at the steel yield initiation point ($M^{(y)}$, Eq. (16)), otherwise, the strengthened beam experiences the concrete cover delamination before the tensile steel yielding.

## 6. Force-Deflection Relationship

The force-deflection relationship of the beams is predicted by using the moment-curvature response at the governing stages derived from the proposed analytical model. For this purpose, it is assumed a linear curvature variation between the beam's sections corresponding to the governing stages. Accordingly, a simply supported beam is divided in distinct regions along the length corresponding to these governing stages, namely, precracking, postcracking and postyielding regions, as shown in Figure 7. The mid-span deflection of the beam is estimated by summing the deflection of each

region ( $\delta_i$ ) in one-half of the beam length ( $L/2$ ) (Figure 8) [25]. The deflection of the each region can be determined by integrating the function, $\chi(x)$, that defines the curvature along the length of this region:

$$\delta_{i(L_i-L_{i+1})} = \int_{Li}^{Li+1} \chi_i(x).x.d(x) \tag{33}$$

where $x$ is a variable along this region, and $L_i$ and $L_{i+1}$ are the distances of the section boundaries of this region to the support.

The negative camber (upward deflection) ( $d^{(ci)}$ ) of the prestressed strengthened beam can be obtained by considering the constant curvature variation due to the effective negative bending moment ( $M_{epre} = \varepsilon_{ef}^{(ci)}.E_f.A_f.e$ ) at both extremities of the bonded length of CFRP reinforcement ( $L_b$ ), as shown in Figure 8a:

$$d^{(ci)} = \int_{L_{ub}}^{L/2} \chi_e^{(ci)}.x.dx = \frac{M_{epre}.L_b(2.L-L_b)}{8.E_c.I_{ucr}} \tag{34}$$

where $\chi_e^{(ci)}$ is the effective initial negative curvature by considering the effective negative bending moment, and $I_{ucr}$ is the moment of inertia of the uncracked section (Appendix A1).

The mid-span deflection of the beam at the concrete crack initiation is calculated adopting the curvature variation along the length of the beam (see Figure 8b) by using Eq. (35). The mid-span deflection corresponding to the concrete and steel decompression points can also be obtained by substituting $\chi^{(cd)}$ and $\chi^{(sd)}$ into Eq. (35) instead of $\chi^{(cr)}$, respectively.

$$d^{(cr)} = \int_0^{b_s} (\frac{\chi^{(cr)}}{b_s}).x^2.dx + \int_{b_s}^{L/2} \chi^{(cr)}.x.dx = \delta_{(0-b_s)}^{(cr)} + \delta_{(b_s-L/2)}^{(cr)} \tag{35}$$

To predict the mid-span deflection at the steel yield initiation stage, the beam length should be divided into the precracking and postcracking regions (Figure 7). In the precracking region, the bending moment is less than the crack initiation moment ( $M^{(cr)}$ ), while the bending moment within the postcracking region is limited to the steel yield

initiation moment ( $M^{(y)}$ ). The mid-span deflection of the beam can be determined by Eq. (36) assuming a linear variation of the curvature between the governing sections, as represented in Figure 8c.

$$d^{(y)} = \int_0^{L_{cr}^{(y)}} (\frac{\chi^{(cr)}}{L_{cr}^{(y)}}).x^2.dx + \int_{L_{cr}^{(y)}}^{b_s} ((\frac{\chi^{(y)} - \chi^{(cr)}}{b_s - L_{cr}^{(y)}}).(x - L_{cr}^{(y)}) + \chi^{(cr)}).x.dx + \int_{b_s}^{L/2} \chi^{(y)}.x.dx = \delta_{(0-L_{cr}^{(y)})}^{(y)} + \delta_{(L_{cr}^{(y)}-b_s)}^{(y)} + \delta_{(b_s-L/2)}^{(y)} \quad (36)$$

where $L_{cr}^{(y)}$ is the length of the precracking region at the steel yield initiation stage (Figure 7 and 8c).

The mid-span deflection of the beam at the ultimate stage can be determined by dividing the beam length in three regions (precracking, postcracking, and postyielding), by considering the trilinear moment-curvature relationship represented in Figure 7. The maximum bending moment within the precracking and postcracking regions are limited by the crack initiation ( $M^{(cr)}$ ) and steel yield initiation ( $M^{(y)}$ ) bending moments, while the ultimate flexural moment of the beam limits the bending moment in the postyielding region. According to the linear variation of the curvature in the three regions of the governing stages, as shown in Figure 8d, Eq. (37) can be considered to calculate the mid-span deflection of the beam corresponding to its flexural capacity.

$$d^{(u)} = \int_0^{L_{cr}^{(u)}} (\frac{\chi^{(cr)}}{L_{cr}^{(u)}}).x^2.dx + \int_{L_{cr}^{(u)}}^{L_y^{(u)}} ((\frac{\chi^{(y)} - \chi^{(cr)}}{L_y^{(u)} - L_{cr}^{(u)}}).(x - L_{cr}^{(u)}) + \chi^{(cr)}).x.dx + \int_{L_y^{(u)}}^{b_s} ((\frac{\chi^{(u)} - \chi^{(y)}}{b_s - L_y^{(u)}}).(x - L_y^{(u)}) + \chi^{(y)}).x.dx + \int_{b_s}^{L/2} \chi^{(u)}.x.dx = \delta_{(0-L_{cr}^{(u)})}^{(u)} + \delta_{(L_{cr}^{(u)}-L_y^{(u)})}^{(u)} + \delta_{(L_y^{(u)}-b_s)}^{(u)} + \delta_{(b_s-L/2)}^{(u)} \quad (37)$$

where $L_{cr}^{(u)}$ is the length of the precracking region, and $L_y^{(u)}$ is the distance of $\chi^{(y)}$ from the support along the beam length at ultimate stage.

It is worth to note that the load ( $P$ ) corresponding to the flexural bending moment at the governing stages for the simply supported beams under four-point loading configuration can be computed by using Eq. (38).

$$P_{(i)} = \frac{4.M_{(i)}}{\left(L - a_L\right)} \quad (38)$$

where $a_L$ is the loading span represented in Figure 3.

## 7. Assessment of Predictive Performance of the Analytical Approach

### *7.1. Conventional flexural failure modes*

To assess the predictive performance of the proposed analytical model, it is applied on the prediction of the force-deflection relationship of the beams forming three experimental programs conducted by Rezazadeh et al. [13], Badawi and Soudki [11], and El-Hacha and Gaafar [12]. These experimental programs are composed of RC beams strengthened with prestressed NSM CFRP reinforcement failed by conventional flexural failure modes, and included an unstrengthened RC beam serving as a control beam, as well as a strengthened beam with a non-prestressed NSM CFRP reinforcement. The level of the prestress force applied to the CFRP reinforcement was 20%, 30% and 40% of its nominal tensile strength in series 1 of the tested beams [13], 40% and 60% in series 2 [11], and 20%, 40% and 60% in series 3 [12].

The data defining the geometry and reinforcement details of the three series of the experimental programs is included in Table 1. All beams were simply supported, and were monotonically tested under four-point loading. It is worth to note that the shear reinforcement ratio and spacing of the stirrups in all the RC beams were designed to avoid the shear failure. The average values of the main properties for concrete, longitudinal steel bars and CFRP elements are indicated in Table 2, where the nominal properties of the CFRP reinforcement were supplied by manufacturer. The used epoxy adhesive provided a proper bond in all cases and, therefore, the analytical formulation previously described is applicable.

Two types of failure modes of the tested beams were experimentally observed: concrete crushing; rupture of the CFRP reinforcement (both after yielding of the tensile steel reinforcement). The prevailing failure modes of the beams at the maximum capacity were analytically predicted similar to the ones experienced experimentally (using the critical percentage of the CFRP reinforcement (Eq. 17)), except in the case of the non-prestressed strengthened beam in series 3 (see Table 5). This can be attributed to the value of the compressive strain experimentally observed on the top fiber of concrete (0.0039 [12]) at the CFRP failure, which is higher than the analytical limit assumed for concrete crushing (0.003). The load versus mid-span deflection relationship obtained analytically and registered experimentally for the all beams of series 1, 2, and 3 is compared in the Figure 9, 10, and 11, respectively. A good predictive performance

of the proposed analytical model is achieved for all the tested beams. Tables 3, 4, and 5 compares the values obtained analytically and registered experimentally for the governing stages of the flexural response of the beams, and also include the short-term prestress loss, initial camber, and prevailing conventional failure mode.

In order to evaluate the efficiency of the proposed simplified analytical approach (formed by a trilinear response), the moment-curvature relationship ( $M-\chi$ ) of the non-prestressed and 40% prestressed strengthened beams of the series 3 obtained with this approach is compared to the one determined by using a sectional analysis software developed at University of Minho (DOCROS-Design Of CROss Sections). DOCROS assumes that a plane section remains plane after deformation and perfect bond exists between distinct materials. According to DOCROS, a cross section is divided in horizontal layers, and the thickness and width of each layer is user-defined and depend on the cross-section geometry. DOCROS can analyze sections of irregular shape and size, composed of different types of materials subjected to an axial force and variable curvature. Composite layers are used when more than one material exist at same depth of the cross section. Each layer can have an initial non-null stress in order to simulate a prestress effect. DOCROS has a wide database of constitutive laws for the simulation of monotonic and cyclic behavior of cement based materials, polymer based materials and steel bars. More detailed information about DOCROS can be found in [30].

In the analysis carried out with DOCROS, the cross section of the non-prestressed and 40% prestressed strengthened beams of the series 3 was discretized in horizontal layers of 1 mm thick. Moreover, in the case of the prestressed section, an initial prestrain was applied to the layers corresponding to the CFRP reinforcement in order to simulate the prestress effect.

The behavior of concrete in uniaxial compression was simulated by the stress-strain relationship proposed by CEB-FIP model code [31], while the behavior of concrete in tension was assumed linear up to its tensile strength and the post-cracking residual strength was neglected in order to provide a more realistic comparison with the analytical approach as described by the diagram represented in Figure 12a [7]. To simulate both tension and compression behavior of the steel bars, the stress-strain relationship represented in Figure 12b was used [7]. The tensile behavior of the CFRP reinforcement was assumed linear up to its ultimate tensile strength.

In Figure 13, the predictive performance of the proposed analytical approach in terms of moment-curvature and neutral axis-curvature relationships is assessed by comparing the results obtained experimentally and numerically (DOCROS) for the non-prestressed and 40% prestressed strengthened beams of the series 3. This figure evidences a good predictive performance for the proposed simplified analytical approach. It should be noted that the experimental moment-curvature and neutral axis-curvature relationships of the analyzed beams were determined by using the strains of components along the mid-span cross section of the aforementioned beams reported by [12].

To evaluate the level of accuracy of the proposed analytical approach on the prediction of force-deflection using the $M-\chi$ relationship, the mid-span deflection of the non-prestressed and 40% prestressed strengthened beams of the series 3 was analytically and numerically obtained using the proposed analytical approach and Def-DOCROS software. For this purpose, the $M-\chi$ relationship obtained in section 5 by using the analytical and numerical approaches was used. According to Def-DOCROS software, a statically determinate beam is discretized in Euler-Bernoulli beam elements of 2 nodes. The updated flexural stiffness of each element is determined from the $M-\chi$ relationship of the cross section representative of the element by using a matrix displacement approach described elsewhere [30]. The experimental, analytical, and numerical force-deflection relationships for the aforementioned beams are compared in Figures 13e and 13f, where it is visible that the proposed analytical approach has high level of predictive performance accuracy.

### *7.2. Concrete cover delamination failure mode*

The proposed methodology for the prediction of the ultimate flexural capacity of the NSM CFRP strengthened beams with concrete cover delamination failure, was applied to six NSM CFRP strengthened beams tested by Sharaky et al. [32], Sharaky [33], Al-Mahmoud et al. [34], Barros and Fortes [7] and Barros et al. [35]. The support and loading configuration of the tested beams are schematically represented in Figures 3 and 5a. The geometry, steel and CFRP reinforcement details of the strengthened beams are described in Table 6. Moreover, the main material properties of the tested beams are represented in Table 7. The shear reinforcement ratio and spacing of stirrups were adopted for all the beams in order to avoid the shear failure.

The parameters of local bond-slip relationship for all the tested beams were adopted similar to the corresponding values considered by [28]: $\tau_{max} = 20.1\text{MPa}$ and $\delta_{max} = 7.12\,\text{mm}$. On the other side, the angle ($\alpha$) between the CFRP

longitudinal axis and generatrices of the concrete fracture surface (semi-pyramid) for all the investigated beams was found equal to 35° by considering the best ultimate flexural capacity for the strengthened beams by using a back analysis of the experimental data. Moreover, this value of $\alpha$ was adopted considering the recommended range by [28] (10°-35°).

The ultimate flexural capacity obtained analytically and registered experimentally for all the tested beams is compared in Table 8, where it can be confirmed that the ultimate flexural capacity of the strengthened beams when failing by the concrete cover delamination was analytically predicted less than the one corresponding to the prevailing conventional flexural failure modes ( $P_{ccd}^{(u)} \le \min(P_{cc}^{(u)}; P_{rc}^{(u)})$ ). Table 8 also indicates the comparison between the concrete tensile fracture capacity ( $F_{cf}$ ) with the tensile strength of CFRP ( $F_{fu}$ ) and resisting bond force ( $F_{rb}$ ) corresponding to the resisting bond length ( $L_{rb}$ ) for each CFRP laminate. A good predictive performance of the analytical approach in terms of the ultimate flexural capacity of the strengthened beams when failing by concrete cover delamination is evidenced by considering the ratio between the analytical and experimental flexural capacity of the tested beams ( $P_{ccd}^{(u)} / P_{ccd}^{(u)\exp}$ ), where this ratio was found between [0.83-1.13] for all the tested beams.

## 8. Conclusions

- In the current study, an analytical approach was developed based on the strain compatibility and principles of static equilibrium to predict the moment-curvature and load-deflection relationships of simply supported beams strengthened with prestressed CFRP reinforcement that can be applied according to the EBR or NSM techniques. The presented formulation assumes that the moment-curvature response of a beam's cross section can be simulated by a trilinear diagram defining precracking, postcracking, and postyielding stages. Two further stages are proposed, namely: concrete and steel decompression stages, to assess the initial effects of the prestress force applied by the CFRP reinforcement. A linear variation is assumed for the curvature along the beam length between the sections corresponding to the governing stages of the beam's response in order to simplify the calculation of the beam's deflection. The flexural capacity of the strengthened beams according to either EBR or NSM techniques is predicted adopting two types of failure modes, comprising yielding of the steel bars in tension followed by either concrete crushing or rupture of the CFRP reinforcement.

- In the case of the NSM technique, a design framework methodology is proposed to obtain the ultimate flexural capacity of the NSM CFRP strengthened beams when failing by concrete cover delamination. Concrete cover delamination is predicted by assessing the possibility of occurring the concrete tensile fracture at the extremities of the CFRP reinforcement in comparison with debonding and rupture of the CFRP failure modes. Finally, the concrete cover delamination is adopted as prevailing failure of the strengthened beams when its ultimate flexural capacity is less than the one corresponding to the occurrence of the conventional flexural failure modes (concrete crushing or rupture of the CFRP reinforcement).
- The results of three experimental programs composed of RC beams strengthened with prestressed NSM CFRP reinforcement, failed by conventional flexural failure modes, were compared with the ones obtained by the proposed analytical approach, and a good predictive performance was determined. Moreover, the results in terms of moment-curvature and force-deflection relationships obtained with the proposed model and by using a computer package (DOCROS and Def-DOCROS software) based on a cross section layer model were compared. The results showed that the proposed analytical approach can accurately simulate the effect of the prestress force on the flexural behavior of the NSM CFRP strengthened beam (by introducing the concrete and steel decompression points as an initial condition to the concrete cracking and steel yielding initiation points of the non-prestressed strengthened beam) compared to the use of a cross section layer model.
- On the other hand, the predictive performance of the proposed methodology for concrete cover delamination failure was evaluated by considering the ultimate load carrying capacity of six NSM CFRP strengthened beams failed according to this failure mode. The proposed formulation provided a good estimate of the ultimate load carrying capacity for concrete cover delamination as prevailing failure mode, resulting the ratio of the analytical and experimental flexural capacity of the tested beams of a mean value and a standard deviation of 0.99 and 0.10, respectively. According to this proposed methodology, by increasing the unbonded length of the CFRP reinforcement at its extremities, the resistance to the occurrence of concrete cover delamination can decrease, while a higher concrete tensile strength and also, a higher concrete cover depth below the tensile steel bars can increase this resistance. On the other side, this resistance is influenced by the distance between the two adjacent CFRPs, as well as distance between the lateral face of the beam's cross section and the nearest CFRP. Accordingly, by adopting a strengthening configuration for consecutive NSM CFRPs according to minimizing the interaction of

the concrete tensile fracture of the adjacent CFRPs can provide the maximum resistance to the occurrence of concrete cover delamination.

**Acknowledgment**

The study reported in this paper is part of the project "PreLami - Performance of reinforced concrete structures strengthened in flexural with an innovative system using prestressed NSM CFRP laminates", with the reference PTDC/ECM/114945/2009. The third author also wishes to acknowledge the scholarship granted by FCT (SFRH/BD/61756/2009). The authors would also like to acknowledge the support provided by S&P, for supplying the adhesives and the laminates, and Casais and CiviTest for the preparation of the beams.

**Notations**

The following symbols are used in this paper:

$A_f$ = area of CFRP reinforcement, mm$^2$.

$A_{groove}$ = area of groove for NSM technique, mm$^2$.

$A_s$ = area of tensile steel bars, mm$^2$.

$A'_s$ = area of compressive steel bars, mm$^2$.

$a_f$ = thickness of CFRP laminate, mm.

$a_L$ = loading span, mm.

$b$ = width of beam, mm.

$b_f$ = width of CFRP laminate, mm.

$b_s$ = shear span, mm.

$c$ = depth of neutral axis from top fiber of concrete at critical point, mm.

$c_c$ = concrete cover for the bottom face of the beam, mm.

$c^{cri}$ = depth of neutral axis from top fiber of concrete at critical CFRP reinforcement ratio, mm.

$d_s$ = distance from centroid of tensile steel bars to top fiber of concrete, mm.

$d'_s$ = distance from centroid of compressive steel bars to top fiber of concrete, mm.

$d_f$ = distance from centroid of CFRP reinforcement to top fiber of concrete, mm.

$e$ = eccentricity of prestress force to centroidal axis of cross section, mm.

$E_c$ = initial Young's modulus of concrete, MPa.

$E_f$ = Young's modulus of CFRP, MPa.

$E_s$ = Young's modulus of longitudinal steel bars, MPa.

$f'_c$ = specified compressive strength of concrete, MPa.

$f_{ct}$ = splitting tensile strength of concrete, MPa.

$f_r$ = flexural tensile strength of concrete, MPa.

$F_{cf}$ = resistance of the concrete fracture surface for each CFRP laminate, N.

$F_{fu}$ = tensile strength of CFRP, N.

$F_{pre}$ = prestress force applied to CFRP reinforcement, N.

$F_{rb}$ = maximum value of the force transferable through the resisting bond length, N.

$f_{sy}$ = yield strength of longitudinal tensile steel bar, MPa.

$h$ = height of beam, mm.

$I_{ucr}$ = moment of inertia of uncracked section of beam, $mm^4$.

$L$ = beam span, mm.

$L_b$ = bonded length of CFRP reinforcement, mm.

$L_{rb}$ = resisting bond length, mm.

$M_{epre}$ = effective negative bending moment due to prestress force, N-mm.

$M$ = flexural moment of beam, N-mm.

$N$ = number of the longitudinal CFRP laminates.

*N.A.* = neutral axis of beam.

$n_f$ = modular ratio of CFRP laminate to concrete, $E_f/E_c$.

$n_s$ = modular ratio of steel reinforcement to concrete, $E_s/E_c$.

$P$ = external load of beam at critical point, N.

$s_f$ = spacing of the two adjacent CFRP laminates, mm.

$s'_f$ = distance between the laminate and the nearest beam edge, mm.

$y_i$ = distance between top fiber of concrete to centroidal axis of uncracked cross section, mm.

$\alpha$ = angle between axis and generatrices of the concrete fracture surface (semi-pyramid).

$\alpha_1$ = multiplier on $f'_c$ to determine intensity of an equivalent rectangular stress distribution.

$\beta_1$ = ratio of depth of equivalent rectangular stress block to the depth of neutral axis.

$\delta_{max}$ = maximum slip of local bond stress-slip relationship, mm.

$\varepsilon_c$ = strain level in concrete, mm/mm.

$\varepsilon'_c$ = strain of unconfined concrete corresponding to $f'_c$, mm/mm.

$\varepsilon_{cc}$ = strain at top extreme fiber of concrete at critical point, mm/mm.

$\varepsilon_{ct}$ = strain at bottom extreme fiber of concrete at critical point, mm/mm.

$\varepsilon_{cu}$ = maximum compressive strain in concrete which is 0.003.

$\varepsilon_{ef}$ = effective tensile strain of CFRP reinforcement at critical point, mm/mm.

$\varepsilon_{fu}$ = ultimate tensile strain of CFRP reinforcement, mm/mm.

$\varepsilon_{lf}$ = short-term prestrain loss in CFRP reinforcement, mm/mm.

$\varepsilon_{fp}$ = prestrain in CFRP reinforcement, mm/mm.

$\varepsilon_s$ = strain in longitudinal tensile steel bar at critical point, mm/mm.

$\varepsilon'_s$ = strain in longitudinal compressive steel bar at critical point, mm/mm.

$\varepsilon_{sy}$ = strain in longitudinal tensile steel bars corresponding to its yield strength, mm/mm.

$\rho_f^{(cri)}$ = critical percentage of CFRP reinforcement, $mm^2/mm.mm$.

$\tau_{max}$ = maximum shear stress of local bond stress-slip relationship, MPa.

$\chi$ = curvature of beam at critical point.

## Appendix A1

Distance from the centroidal axis of beam cross section ( $y_i$ ) and moment of inertia of uncracked section ( $I_{ucr}$ ) can be obtained as follows:

$$y_i = \frac{\sum_{i=1}^{n} A_i.d_i}{\sum_{i=1}^{n} A_i} = \frac{b.h^2/2 - A_{groove}.d_f + A'_s.(n_s-1).d'_s + A_s.(n_s-1).d_s + A_f.n_f.d_f}{b.h - A_{groove} + A'_s.(n_s-1) + A_s.(n_s-1) + A_f.n_f} \quad \text{(A1)-a}$$

$$I_{ucr} = \frac{1}{12}.b.h^3 + b.h.\left(y_i - \frac{h}{2}\right)^2 - A_{groove}.\left(d_f - y_i\right)^2 + A_s^{'}.\left(n_s - 1\right).\left(y_i - d_s^{'}\right)^2 + A_s.\left(n_s - 1\right).\left(d_s - y_i\right)^2 + A_f.n_f.\left(d_f - y_i\right)^2 \quad \text{(A1)-b}$$

where $A_{groove}$ is area of the groove for NSM technique, $n_s$ and $n_f$ are the modular ratio of steel and CFRP reinforcement to concrete, respectively.

Tensile strain at the top fiber ( $\varepsilon_{cc}^{(ci)}$ ) and compressive strain at the bottom fiber ( $\varepsilon_{ct}^{(ci)}$ ) of concrete are:

$$\varepsilon_{cc}^{(ci)} = \frac{\left(\left(\frac{F_{pre}.e.y_i}{I_{ucr}}\right) - \left(\frac{F_{pre}}{b.h}\right)\right)}{E_c} \quad \text{(A1)-c}$$

$$\varepsilon_{ct}^{(ci)} = \frac{\left(\left(\frac{F_{pre}.e.(h - y_i)}{I_{ucr}}\right) + \left(\frac{F_{pre}}{b.h}\right)\right)}{E_c} \quad \text{(A1)-d}$$

In fact, due to the short-term prestrain loss in the CFRP reinforcement ( $\varepsilon_{ef}^{(ci)}$ obtained from Eq. (4)) after the release of the prestress force, effective prestress force ( $F_{epre} = E_f.\varepsilon_{ef}^{(ci)}.A_f$ ) should be used in Eqs. (A1)-c and (A1)-d instead of the applied prestress force ( $F_{pre} = E_f.\varepsilon_{fp}.A_f$ ), while the effect of this short-term prestrain loss was neglected to determine the tensile strain at the top fiber and compressive strain at the bottom fiber of concrete in order to simplify the calculation procedure.

Strains in the compressive and tensile steel bars can be obtained by:

$$\varepsilon_s^{'(ci)} = \frac{\varepsilon_{cc}^{(ci)}.\left(c^{(ci)} - d_s^{'}\right)}{c^{(ci)}} \quad \text{(A2)-a}$$

$$\varepsilon_s^{(ci)} = \frac{\varepsilon_{cc}^{(ci)}.\left(d_s - c^{(ci)}\right)}{c^{(ci)}} \quad \text{(A2)-b}$$

It should also be noted that Eqs. (A1)-c - (A2)-b are derived by assuming no cracking occurs after the release of the prestress force (Figures 3 and 14) [25].

**Appendix A2**

Strains in the constituent materials along the depth of the cross section (longitudinal top ( $\varepsilon_s^{'}$ ) and bottom ( $\varepsilon_s$ ) steel bars, CFRP reinforcement ( $\varepsilon_f$ ), and bottom fiber of concrete ( $\varepsilon_{ct}$ )) at concrete decompression (cd) and steel decompression (sd) points are:

$$\varepsilon_s^{'(cd)} = \frac{\varepsilon_{cc}^{(cd)}.\left(h - d_s^{'}\right)}{h} \quad \text{(A3)-a}$$

$$\varepsilon_s^{(cd)} = \frac{\varepsilon_{cc}^{(cd)}.\left(h - d_s\right)}{h} \quad \text{(A3)-b}$$

$$\varepsilon_f^{(cd)} = \frac{\varepsilon_{cc}^{(cd)}.\left(h - d_f\right)}{h} \quad \text{(A3)-c}$$

$$\varepsilon_s^{'(sd)} = \frac{\varepsilon_{cc}^{(sd)}.\left(d_s - d_s^{'}\right)}{d_s} \quad \text{(A4)-a}$$

$$\varepsilon_{ct}^{(sd)} = \frac{\varepsilon_{cc}^{(sd)}.\left(h - d_s\right)}{d_s} \quad \text{(A4)-b}$$

$$\varepsilon_f^{(sd)} = \frac{\varepsilon_{cc}^{(sd)}.\left(d_f - d_s\right)}{d_s} \quad \text{(A4)-c}$$

Effective tensile strains for the prestressed CFRP reinforcements are as follows:

$$\varepsilon_{ef}^{(cd)} = \varepsilon_{fp} + \varepsilon_f^{(cd)} \quad \text{(A5)-a}$$

$$\varepsilon_{ef}^{(sd)} = \varepsilon_{fp} + \varepsilon_f^{(sd)} \quad \text{(A5)-b}$$

Both concrete and steel decompression points are assumed to occur before the concrete crack initiation point by considering an uncracked section (Figures 3 and 15).

**Appendix A3**

$$\varepsilon_{ctb}^{(cr)} = \varepsilon_{ct} = \frac{f_r}{E_c} \rightarrow \varepsilon_{ccb}^{(cr)} = \frac{\varepsilon_{ctb}^{(cr)}.y_i}{\left(h - y_i\right)} \quad \text{(A6)-a}$$

Strain components of the longitudinal steel bars in compression ( $\varepsilon_{sb}^{'(cr)}$ ) and in tension ( $\varepsilon_{sb}^{(cr)}$ ), and CFRP reinforcement ( $\varepsilon_{fb}^{(cr)}$ ) can be obtained by:

$$\varepsilon_{sb}^{'(cr)} = \frac{\varepsilon_{ccb}^{(cr)}.\left(y_i - d_s^{'}\right)}{y_i} \quad \text{(A6)-b}$$

$$\varepsilon_{sb}^{(cr)} = \frac{\varepsilon_{ccb}^{(cr)}.\left(d_s - y_i\right)}{y_i} \quad \text{(A6)-c}$$

$$\varepsilon_{fb}^{(cr)} = \frac{\varepsilon_{ccb}^{(cr)}.\left(d_f - y_i\right)}{y_i} \quad \text{(A6)-d}$$

Uncracked section was assumed to determine Eqs. (A6)-a - (A6)-d (Figures 2a and 3).

**Appendix A4**

By adopting the principles of static equilibrium at the steel yield initiation point (Figure 2b):

$$\frac{1}{2}\varepsilon_{ccb}^{(y)}.E_c.c_b^{(y)}.b + A_s^{'}.\varepsilon_{sb}^{'(y)}.E_s - A_s.\varepsilon_{sb}^{(y)}.E_s - A_f.\varepsilon_{fb}^{(y)}.E_f = 0 \quad \text{(A7)}$$

where compressive strains at the top fiber of concrete ( $\varepsilon_{ccb}^{(y)}$ ) and longitudinal top steel bars ( $\varepsilon_{sb}^{'(y)}$ ), and tensile strain in the CFRP reinforcement ( $\varepsilon_{fb}^{(y)}$ ) can be obtained by:

$$\varepsilon_{ccb}^{(y)} = \frac{\varepsilon_{sb}^{(y)}.c_b^{(y)}}{\left(d_s - c_b^{(y)}\right)} \quad \text{(A8)-a}$$

$$\varepsilon_{sb}^{'(y)} = \frac{\varepsilon_{sb}^{(y)}.\left(c_b^{(y)} - d_s^{'}\right)}{\left(d_s - c_b^{(y)}\right)} \le \varepsilon_{sy} \quad \text{(A8)-b}$$

$$\varepsilon_{fb}^{(y)} = \frac{\varepsilon_{sb}^{(y)}.\left(d_f - c_b^{(y)}\right)}{\left(d_s - c_b^{(y)}\right)} \quad \text{(A8)-c}$$

The equations represented in this section are determined by assuming a cracked section, and also the resistance of concrete in tension is neglected (Figures 2b and 3) [25].

**Appendix A5**

The critical percentage of CFRP reinforcement ( $\rho_f^{(cri)}$ ) can be determined assuming simultaneous tension and compression failures (Figure 16a):

$$\alpha_1.f_c^{'}.\beta_1.c^{(cri)}.b + A_s^{'}.\varepsilon_s^{'(cri)}.E_s - A_s.f_{sy} - A_f^{(cri)}.\varepsilon_{fu}.E_f = 0 \quad \text{(A9)}$$

where the neural axis depth ( $c^{(cri)}$ ) and strain components in the longitudinal top ( $\varepsilon_s^{'(cri)}$ ) and bottom ( $\varepsilon_s^{(cri)}$ ) steel bars at simultaneous tension and compression failures are:

$$c^{(cri)} = \frac{d_f.\varepsilon_{cu}}{((\varepsilon_{fu} - \varepsilon_{fp}) + \varepsilon_{cu})} \quad \text{(A10)}$$

$$\varepsilon_s^{'(cri)} = \frac{\varepsilon_{cu}.\left(c^{(cri)} - d_s^{'}\right)}{c^{(cri)}} \le \varepsilon_{sy} \quad if\ not\ \rightarrow \varepsilon_s^{'(cri)}.E_s = f_{sy} \quad \text{(A11)-a}$$

$$\varepsilon_s^{(cri)} = \frac{\varepsilon_{cu}\left(d_s - c^{(cri)}\right)}{c^{(cri)}} \ge \varepsilon_{sy} \rightarrow \varepsilon_s^{(cri)}.E_s = f_{sy} \quad \text{(A11)-b}$$

The equations of this section are derived by assuming a cracked section, and also the resistance of concrete in tension is neglected (Figures 3 and 16a) [25].

*Concrete Crushing*

From the strain profile of the cross section when the concrete crushing occurs (Figure 16b):

$$\alpha_1.f_c^{'}.\beta_1.c_{cc}^{(u)}.b + A_s^{'}.\varepsilon_{s,cc}^{'(u)}.E_s - A_s.f_{sy} - A_f.E_f.\varepsilon_{f,cc}^{(u)} = 0 \quad \text{(A12)}$$

where compressive strains in the longitudinal top steel bars ( $\varepsilon_{s,cc}^{'(u)}$ ), and tensile strain in the CFRP reinforcement ( $\varepsilon_{fb,cc}^{(u)}$ ) can be obtained from the following equations:

$$\varepsilon_{s,cc}^{'(u)} = \frac{\varepsilon_{cu}.\left(c_{cc}^{(u)} - d_s^{'}\right)}{c_{cc}^{(u)}} \le \varepsilon_{sy} \quad if\ not\ \rightarrow \varepsilon_{s,cc}^{'(u)}.E_s = f_{sy} \quad \text{(A13)-a}$$

$$\varepsilon_{fb,cc}^{(u)} = \frac{\left(d_f - c_{cc}^{(u)}\right).\varepsilon_{cu}}{c_{cc}^{(u)}} \rightarrow \varepsilon_{f,cc}^{(u)} = \varepsilon_{fb,cc}^{(u)} + \varepsilon_{fp} \le \varepsilon_{fu} \quad \text{(A13)-b}$$

*Rupture of CFRP Reinforcement*

The equilibrium of the internal forces, when the rupture of the CFRP reinforcement occurs, results in the following equation (Figure 16c):

$$\alpha_1.f_c^{'}.\beta_1.c_{rc}^{(u)}.b + A_s^{'}.\varepsilon_{s,rc}^{'(u)}.E_s - A_s.f_{sy} - A_f.f_{fu} = 0 \quad \text{(A14)}$$

where compressive strains at the top fiber of concrete ( $\varepsilon_{cc,rc}^{(u)}$ ) and in the longitudinal top steel bars ( $\varepsilon_{s,rc}^{'(u)}$ ), and tensile strain in the CFRP reinforcement ( $\varepsilon_{fb,rc}^{(u)}$ ) can be obtained by:

$$\varepsilon_{cc,rc}^{(u)} = \frac{\varepsilon_{fb,rc}^{(u)}.c_{rc}^{(u)}}{\left(d_f - c_{rc}^{(u)}\right)} \quad \text{(A15)-a}$$

$$\varepsilon_{fb,rc}^{(u)} = \varepsilon_{fu} - \varepsilon_{fp} \quad \text{(A15)-b}$$

$$\varepsilon_{s,rc}^{'(u)} = \frac{\varepsilon_{fb,rc}^{(u)}.\left(c_{rc}^{(u)} - d_s^{'}\right)}{\left(d_f - c_{rc}^{(u)}\right)} \le \varepsilon_{sy} \quad if\ not \rightarrow \varepsilon_{s,rc}^{'(u)}.E_s = f_{sy} \quad \text{(A16)}$$

**References**


[1] ACI-440.2R. Guide for the Design and Construction of Externally Bonded FRP Systems for Strengthening Concrete Structures. *American Concrete Institute*, 2008.

[2] CAN/CSA-S6-00. Canadian Highway Bridge Design Code. Toronto, Canada, 2000.

[3] ISIS Canadian Network of Centres Excellence. Prestressing Concrete Structures with Fibre Reinforced Polymers. 9. *Department of Civil Engineering, University of Calgary*, Contributor: Raafat El-Hacha, 2007; p. 14.

[4] Dias, S., and Barros, J. Shear Strengthening of RC Beams with NSM CFRP Laminates: Experimental Research and Analytical Formulation. *Composite Structures*. 2012; 99:477-90.

[5] Rabinovitch, O., and Frosting, Y. Experimental and Analytical Comparison of RC Beams Strengthened with CFRP Composites. *Composite Part B: Engineering*. 2003; 34:14.

[6] El-Hacha, R., and Rizkalla, S. Near-Surface-Mounted Fiber-Reinforced Polymer Reinforcements for Flexural Strengthening of Concrete Structures. *ACI Structural Journal*. 2004; 101(5):717-26.

[7] Barros, J., and Fortes, A. Flexural Strengthening of Concrete Beams with CFRP Laminates Bonded into Slits. *Cement and Concrete Composites*. 2005; 27(4) p:471-80.

[8] De Lorenzis, L., and Teng, J. Near-Surface Mounted FRP Reinforcement: an Emerging Technique for Structural Strengthening. *Composite Part B: Engineering,* 2007;39(2):119-49.

[9] Bilotta, A., Ceroni, F., Nigro, E., and Pecce, M. Bond Behavior of FRP NSM Systems in Concrete Elements. *composite Part B: Engineering*, 2012;43(2):99-109.

[10] Nordin, H., and Taljsten, B. Concrete Beams Strengthened with Prestressed Near Surface Mounted CFRP. *Journal of Composites for Construction*. 2006; 60-8.

[11] Badawi, M., and Soudki, K. Flexural Strengthening of RC Beams with Prestressed NSM CFRP Rods-Experimental and Analytical Investigation. *Construction and Building Materials*. 2009; 3292-300.

[12] El-Hacha, R., and Gaafar, M. Flexural Strengthening of Reinforced Concrete Beams Using Prestressed Near-Surface-Mounted CFRP Bars. *PCI Journal*. 2011.

[13] Rezazadeh, M., Costa, I., and Barros, J. Influence of Prestress Level on NSM CFRP Laminates for the Flexural Strengthening of RC Beams. *Composite Structures*. 2014; 116:489-500.

[14] Hajihashemi, A., Mostofinejad, D., and Azhari, M. Investigation of RC Beams Strengthened with Prestressed NSM CFRP Laminates. *Journal of Composites for Construction (ASCE)*. 2011; 15(6.).

[15] Rezazadeh, M., and Barros, J. A New Hybrid Methodology According to Near Surface Mounted Carbon Fiber Reinforced Polymer Technique for the Flexural Strengthening of Reinforced Concrete Beams. *Reinforced Plastics and Composites*, 2014; DOI: 10.1177/0731684414551374.

[16] Xue, W., Tan, Y., and Zeng, L. Flexural Response Predictions of Reinforced Concrete Beam Strengthened with Prestressed CFRP plates. *Composite Structures*. 2009; 92:612-22.

[17] Teng, J., Smith, S., Yao, J., and Chen, J. Intermediate Crack-induced Debonding in RC Beams and Slabs. *Construction and Building Materials*. 2003; 17:447-62.

[18] Gao, B., Leung, C., Kim, J. Prediction of concrete cover separation failure for RC beams strengthened with CFRP strips. *Engineering Structures.* 2004; 27:177-89.

[19] Xiong, G., Jiang, X., Liu, J., and Chen, L. A Way for Preventing Tension Delamination of Concrete Cover in Midspan of FRP Strengthened Beams. *Construction and Building Materials*. 2007; 21:402–8..

[20] Alwis, W. Trilinear Moment-Curvature Relationship for Reinforced Concrete Beams. *ACI Structural Journal*. 1990; 8.

[21] Saqan, E., and Rasheed, H. Simplified Nonlinear Analysis to Compute Neutral Axis Depth in Prestressed Concrete Regtangular Beams. *Journal of the Franklin Institute.* 2010; 348:1588-604.

[22] El-Mihilmy, M, and Tedesco, W. Deflection of Reinforced Concrete Beams Strengthened with Fiber-Reiforced Polymer (FRP) Plates. *ACI Structural Journal*. 2000; 97(5):8.

[23] Rasheed, H., Charkas, H., and Melhem, H. Simplified Nonlinear Analysis of Strengthened Concrete Beams based on a Rigorous Approach. *Journal of Structural Engineering (ASCE)*. 2004; 130(7.).

[24] Barros, J., and Dalfre, G. A Model for the Prediction of the Behaviour of Countinuous RC Slabs Flexurally Strengthened with CFRP Systems. In: Proceedings of *FRPRCS 11*. Guimaraes, Portugal., Conference, Conference 2013.

[25] Rezazadeh, M., Barros, J., and Costa, I. Analytical Model for the Prediction of the Behavior of RC Beams Flexurally Strengthened with Prestressed NSM CFRP Laminates. *Report nº 2014-DEC/E-04*, *University of Minho,* 2014.

[26] ACI-318M-08. Building Code Requirements for Structural Concrete. *American Concrete Institute*, 2008.

[27] Barros, J., and Kotynia, R. Possibilities and Challenges of NSM for the Flexural Strengthening of RC Structures. Proceedings of *Fourth International Conference on FRP Composites in Civil Engineering.* Zurich, Switzerland, 2008.

[28] Bianco, V., Monti, G., and Barros, J. Design Formula to Evaluate the NSM FRP Strips Shear Strength Contribution to a RC Beam. *Composite Part B: Engineering*. 2014; 56:960-71.

[29] Bianco, V. Shear Strengthening of RC Beams by Means of NSM CFRP Strips: Experimental Evidence and Analytical Modeling. *PhD thesis, Sapienza University of Rome.* 2008.

[30] Varma, R K. Numerical Models for the Simulation of the Cyclic Behaviour of RC Structures Incorporating New Advanced Materials. *PhD thesis, University of Minho, Portugal*, 2012.

[31] CEB-FIP Model Code. Comite Euro-International du Beton, . Bulletin d'Information n 213/214,1993.

[32] Sharaky, I., Torres, L., Comas, J., and Barris, C. Flexural Response of Reinforced Concrete (RC) Beams Strengthened with Near Surface Mounted (NSM) Fibre Reinforced Polymer (FRP) Bars. *Composite Structures*. 2014; 109.

[33] Sharaky, I. A Study of the Bond and Flexural Behaviour of Reinforced Concrete Elements Strengthened with Near Surface Mounted (NSM) FRP Reinforcement. *PhD thesis, Spain: University of Girona.* 2013.

[34] Al-Mahmoud, F., Castel, A., Francois, R., and Tourneur, C. Strengthening of RC Members with Near-Surface-Mounted CFRP Rods. *Composite Structures*. 2009; 91.

[35] Barros, J., Dias, S., and Lima, J. Efficacy of CFRP-based Techniques for the Flexural and Shear Strengthening of Concrete Beams. *Cement and Concrete Composites*. 2007; 29(3).

Table 1: Geometry and reinforcement details of the beam series [11-13]

| Beam series | No. | $L$ (mm) | $a_L$ (mm) | $b_s$ (mm) | $b$ (mm) | $h$ (mm) | $d'_s$ (mm) | $d_s$ (mm) | $d_f$ (mm) | $A'_s$ (mm$^2$) | $A_s$ (mm$^2$) | $A_f$ (mm$^2$) | *groove size* (mm$^2$) |
|---|---|---|---|---|---|---|---|---|---|---|---|---|---|
| Series 1 [13] | 5 | 2200 | 400 | 900 | 150 | 300 | 25 | 265 | 288 | 157.1 (2φ10) | 157.1 (2φ10) | 28 CFRP laminate (1.4×20) | 144 6×24 |
| Series 2 [11] | 4 | 3300 | 1100 | 1100 | 152 | 254 | 35 | 220 | 241.5 | 197 (2φ11.2) | 353.4 (2φ15) | 70.9 CFRP bar (1φ9.5) | 375 15×25 |
| Series 3 [12] | 5 | 5000 | 1000 | 2000 | 200 | 400 | 35 | 343 | 387.5 | 200.6 (2φ11.3) | 603.2 (3φ16) | 63.6 CFRP bar (1φ9) | 500 20×25 |

Table 2: Main properties for concrete, steel and CFRP reinforcements [11-13]

| Beam series | *concrete* | *Steel reinforcement* | | | *CFRP reinforcement* | | *nominal CFRP properties* | |
|---|---|---|---|---|---|---|---|---|
| | $f'_c$ (MPa) | $f_{sy}$ (MPa) | $f_{su}$ (MPa) | $E_s$ (GPa) | $f_{fu}$ (MPa) | $E_f$ (GPa) | $f_{fu(n)}$ (MPa) | $E_{f(n)}$ (GPa) |
| Series 1 [13] | 32 | 585 | 656 | 208 | 1922 | 164 | 2000 | 150 |
| Series 2 [11] | 45 | 440 | 560 | 190 | 1970 | 136 | 1970 | 136 |
| Series 3 [12] | 40 | 475 | - | 200 | 2167 | 130 | 2068 | 124 |

Table 3: Experimental and analytical values of the governing stages of the flexural response for the RC beams of the series 1 [13]

| *RC beams* | *Result* | $d^{ci}$ *(mm)* | $\varepsilon_{lf}^{ci}$ *(%)* | $P^{cd}$ *(kN)* | $d^{cd}$ *(mm)* | $P^{sd}$ *(kN)* | $d^{sd}$ *(mm)* | $P^{cr}$ *(kN)* | $d^{cr}$ *(mm)* | $P^{y}$ *(kN)* | $d^{y}$ *(mm)* | $P^{u}$ *(kN)* | $d^{u}$ *(mm)* | *Failue Mode* |
|---|---|---|---|---|---|---|---|---|---|---|---|---|---|---|
| Control | Exper | - | - | - | - | - | - | 13.81 | 0.30 | 49.70 | 5.87 | 61.46 | 45.70 | CC |
| | Analy | | | | | | | 17.70 | 0.37 | 52.40 | 5.30 | 53.64 | 30.43 | CC |
| Non prestressed | Exper | 0 | 0 | 0 | 0 | 0 | 0 | 17.01 | 0.35 | 60.32 | 5.93 | 92.97 | 24.46 | RC |
| | Analy | | | | | | | 17.85 | 0.37 | 60.24 | 5.53 | 86.60 | 18.11 | RC |
| 20% prestressed | Exper | -0.08 | 0.40 | - | - | 7.10 | 0.17 | 22.14 | 0.46 | 68.69 | 6.14 | 94.00 | 19.36 | RC |
| | Analy | -0.10 | 1.20 | 5.71 | 0.11 | 6.00 | 0.13 | 23.59 | 0.49 | 66.37 | 5.41 | 86.34 | 13.80 | RC |
| 30% prestressed | Exper | -0.18 | 1.30 | - | - | 15.5 | 0.36 | 23.04 | 0.55 | 72.52 | 6.52 | 95.16 | 16.92 | RC |
| | Analy | -0.15 | 1.20 | 8.20 | 0.17 | 8.60 | 0.18 | 26.08 | 0.54 | 68.88 | 5.35 | 86.10 | 12.07 | RC |
| 40% prestressed | Exper | - | 1.90 | - | - | 18.10 | 0.25 | 25.08 | 0.47 | 74.16 | 5.34 | 87.45 | 10.15 | RC |
| | Analy | -0.20 | 1.20 | 10.68 | 0.22 | 11.21 | 0.24 | 28.46 | 0.59 | 71.48 | 5.30 | 85.82 | 10.42 | RC |

- $d^{ci}$ is initial deflection due to prestressing force;
- $\varepsilon_{lf}^{ci}$ is the short-term losses of the tensile strain of the prestressed laminate after releasing;
- $P^{cd}$ is the load at concrete decompression point, and $d^{cd}$ its corresponding deflection;
- $P^{sd}$ is the load at steel decompression point, and $d^{sd}$ its corresponding deflection;
- $P^{cr}$ is the load at cracking initiation, and $d^{cr}$ its corresponding deflection;
- $P^{y}$ is the load at yield initiation of the longitudinal tensile bars, and $d^{y}$ its corresponding deflection;
- $P^{u}$ is the ultimate load, and $d^{u}$ its corresponding deflection;
- *CC* is concrete crushing, and *RC* is rupture of CFRP

Table 4: Experimental and analytical values of the governing stages of the flexural response for the RC beams of the series 2 [11]

| *RC beams* | *Result* | $d^{ci}$ *(mm)* | $\varepsilon_{lf}^{ci}$ *(%)* | $P^{cd}$ *(kN)* | $d^{cd}$ *(mm)* | $P^{sd}$ *(kN)* | $d^{sd}$ *(mm)* | $P^{cr}$ *(kN)* | $d^{cr}$ *(mm)* | $P^{y}$ *(kN)* | $d^{y}$ *(mm)* | $P^{u}$ *(kN)* | $d^{u}$ *(mm)* | *Failue Mode* |
|---|---|---|---|---|---|---|---|---|---|---|---|---|---|---|
| Control | Exper | - | - | - | - | - | - | 10.20 | 1.86 | 55.10 | 23.50 | 64.30 | 85.30 | CC |
| | Analy | | | | | | | 13.13 | 1.29 | 55.80 | 17.60 | 57.43 | 95.00 | CC |
| Non prestressed | Exper | 0 | 0 | 0 | 0 | 0 | 0 | 10.92 | 1.76 | 69.50 | 26.03 | 96.50 | 65.49 | CC |
| | Analy | | | | | | | 12.90 | 1.14 | 65.26 | 18.43 | 102.23 | 64.80 | CC |
| 40% prestressed | Exper | - | - | - | - | - | - | 30.09 | 4.34 | 95.00 | 25.82 | 115.25 | 48.34 | RC |
| | Analy | -1.21 | 2.48 | 17.85 | 1.55 | 19.85 | 1.73 | 30.92 | 2.70 | 86.38 | 17.71 | 113.35 | 47.13 | RC |
| 60% prestressed | Exper | - | - | - | - | - | - | 40.00 | 5.05 | 105.00 | 25.72 | 112.26 | 32.89 | RC |
| | Analy | -1.81 | 2.48 | 26.78 | 2.33 | 29.78 | 2.61 | 39.85 | 3.51 | 96.31 | 17.70 | 112.08 | 32.96 | RC |

Table 5: Experimental and analytical values of the governing stages of the flexural response for the RC beams of the series 3 [12]

| *RC beams* | *Result* | $d^{ci}$ *(mm)* | $\varepsilon_{lf}^{ci}$ *(%)* | $P^{cd}$ *(kN)* | $d^{cd}$ *(mm)* | $P^{sd}$ *(kN)* | $d^{sd}$ *(mm)* | $P^{cr}$ *(kN)* | $d^{cr}$ *(mm)* | $P^{y}$ *(kN)* | $d^{y}$ *(mm)* | $P^{u}$ *(kN)* | $d^{u}$ *(mm)* | *Failue Mode* |
|---|---|---|---|---|---|---|---|---|---|---|---|---|---|---|
| Control | Exper | - | - | - | - | - | - | 12.50 | 1.30 | 78.90 | 25.10 | 83.80 | 109.90 | CC |
| | Analy | | | | | | | 21.54 | 1.64 | 86.90 | 22.20 | 89.56 | 143.60 | CC |
| Non prestressed | Exper | 0 | 0 | 0 | 0 | 0 | 0 | 18.40 | 1.60 | 90.20 | 25.30 | 136.40 | 114.50 | RC |
| | Analy | | | | | | | 21.45 | 1.53 | 94.49 | 22.15 | 136.26 | 88.80 | CC |
| 20% prestressed | Exper | -0.50 | 6.26 | - | - | - | - | 22.10 | 1.50 | 105.70 | 27.70 | 141.00 | 92.50 | RC |
| | Analy | -0.47 | 1.19 | 7.59 | 0.52 | 8.35 | 0.60 | 29.06 | 2.07 | 104.46 | 22.29 | 140.13 | 76.50 | RC |
| 40% prestressed | Exper | -0.60 | 6.03 | - | - | - | - | 27.90 | 1.70 | 114.50 | 28.60 | 141.70 | 79.30 | RC |
| | Analy | -0.94 | 1.19 | 15.19 | 1.10 | 16.70 | 1.20 | 36.65 | 2.61 | 112.81 | 22.02 | 139.45 | 57.70 | RC |
| 60% prestressed | Exper | -1.30 | 10.10 | - | - | - | - | 34.40 | 2.40 | 117.70 | 28.20 | 134.70 | 49.70 | RC |
| | Analy | -1.42 | 1.19 | 22.94 | 1.64 | 25.22 | 1.78 | 44.40 | 3.17 | 121.33 | 21.87 | 138.43 | 40.22 | RC |

Table 6: Geometry, steel and CFRP reinforcement details of the tested beams [7, 32-35]

| Tested beams | $L_b$ (mm) | $L_{ub}$ (mm) | $a_L$ (mm) | $b_s$ (mm) | $b$ (mm) | $h$ (mm) | $d'_s$ (mm) | $d_s$ (mm) | $d_f$ (mm) | $A'_s$ (mm) | $A_s$ (mm) | $A_f$* (mm) | $s_f$ (mm) | $s'_f$ (mm) |
|---|---|---|---|---|---|---|---|---|---|---|---|---|---|---|
| by [32] | 2000 | 200 | 800 | 800 | 160 | 280 | 40 | 240 | 272 | 2φ8 | 2φ12 | 2bφ8 | 80 | 40 |
| by [33] | 2000 | 200 | 800 | 800 | 160 | 280 | 40 | 240 | 270 | 2φ8 | 2φ12 | 1bφ8 & 2L:1.4x20 | 45.5 | 34.5 |
| by [34] | 2100 | 350 | 1200 | 800 | 150 | 280 | 40 | 240 | 274 | 2φ6 | 2φ12 | 2bφ6 | 88 | 31 |
| by [7]-a | 1400 | 50 | 500 | 500 | 100 | 177 | 25 | 152 | 171 | 2φ8 | 3φ6 | 2L:1.4x10 | 30 | 35 |
| by [7]-b | 1400 | 50 | 500 | 500 | 100 | 175 | 25 | 152 | 169 | 2φ8 | 2φ6 & 1φ8 | 2L:1.4x10 | 30 | 35 |
| by [35] | 800 | 50 | 300 | 300 | 120 | 170 | 21 | 149 | 164 | 2φ6.5 | 2φ6.5 | 2L:1.4x10 | 40 | 40 |

* Two types of CFRP reinforcement were used: CFRP round bar (b) and CFRP laminate (L)

Table 7: Main properties for the concrete, steel and CFRP reinforcements [7, 32-35]

| Tested beams | *concrete* | *Steel reinforcement* | | | *CFRP reinforcement* | |
|---|---|---|---|---|---|---|
| | $f'_c$ (MPa) | $f_{sy}$ (MPa) | $f_{su}$ (MPa) | $E_s$ (GPa) | $f_{fu}$ (MPa) | $E_f$ (GPa) |
| by [32] and [33] | 32 | 545 | 624 | 205 | 2350 | 170 |
| by [34] | 37 | 600 | - | 210 | 1875 | 146 |
| by [7] | 46 | 730 | 800 | 200 | 2740 | 159 |
| by [35] | 52 | 627 | 765 | 200 | 2740 | 159 |

Table 8: Experimental and analytical values of the ultimate flexural capacity of the tested beams [7, 32-35]

| Tested beams | $\alpha$ (°) | $L_{rb}$ (mm) | $F_{cf}$ (kN) | $F_{fu}$ (kN) | $F_{rb}$ (kN) | $F_{cfe}$ (kN) | $P_{cc}^{(u)}$ (kN) | $P_{rc}^{(u)}$ (kN) | $P_{ccd}^{(u)}$ (kN) | $P_{ccd}^{(u)\exp}$ (kN) | $\frac{P_{ccd}^{(u)}}{P_{ccd}^{(u)\exp}}$ |
|---|---|---|---|---|---|---|---|---|---|---|---|
| by [32] | 35 | 57.12 | 10.20 | 117.79 | 24.28 | 20.40 | 164.30 | - | **118.75** | **116.01** | **1.02** |
| by [33] | 35 | 57.12 | 5.80 | 83.29 | 21.89 | 17.40 | 165.39 | - | **99.33** | **118.58** | **0.83** |
| by [34] | 35 | 55.70 | 8.20 | 52.86 | 17.72 | 16.40 | - | 128.29 | **102.56** | **108.12** | **0.94** |
| by [7]-a | 35 | 35.70 | 2.84 | 36.77 | 14.67 | 5.69 | 88.10 | - | **84.46** | **78.50** | **1.07** |
| by [7]-b | 35 | 32.84 | 2.62 | 36.77 | 13.51 | 5.24 | 94.25 | - | **93.09** | **81.91** | **1.13** |
| by [35] | 35 | 29.99 | 3.39 | 36.77 | 12.36 | 6.79 | 108.80 | - | **91.47** | **92.49** | **0.99** |

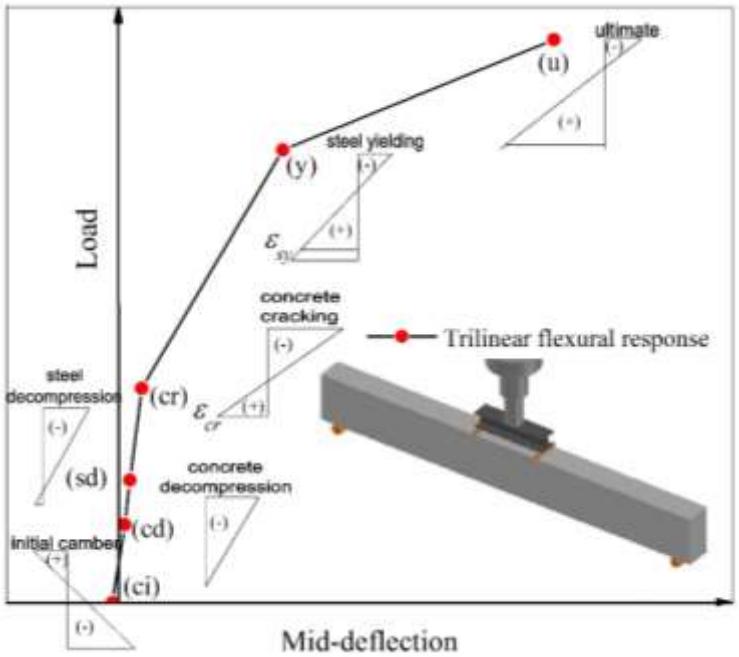


Figure 1: Critical points of the trilinear flexural response of the prestressed strengthened beams

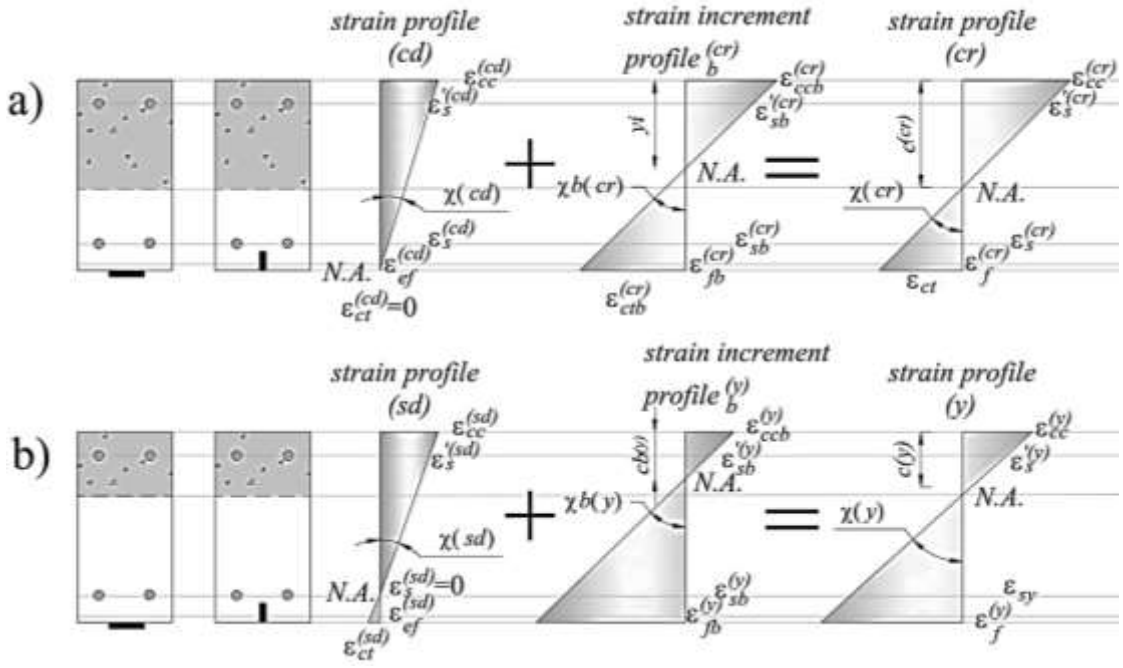


Figure 2: Strain profile of the cross section: a) at concrete crack initiation point (cr), b) at steel yield initiation point (y)

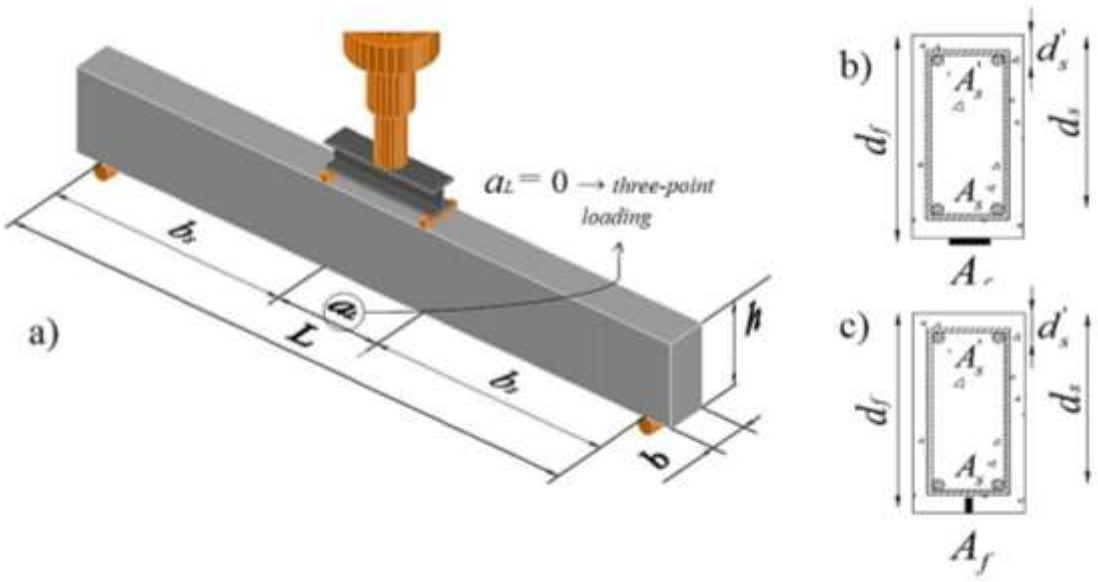


Figure 3: Definition of the geometry and reinforcement configuration for the analytical model: a) geometry of strengthened beam, b) reinforcement details in EBR technique, c) reinforcement details in NSM technique

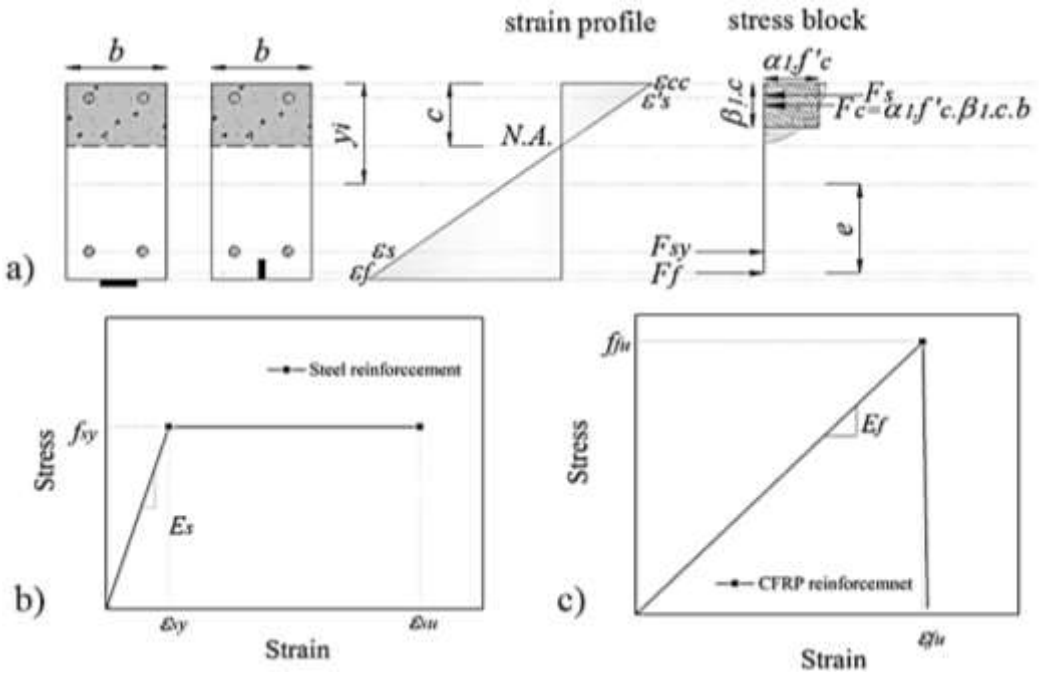


Figure 4: a) Compressive stress block for the concrete in compression, b) stress-strain relationship for the steel, c) stress strain relationship for the CFRP

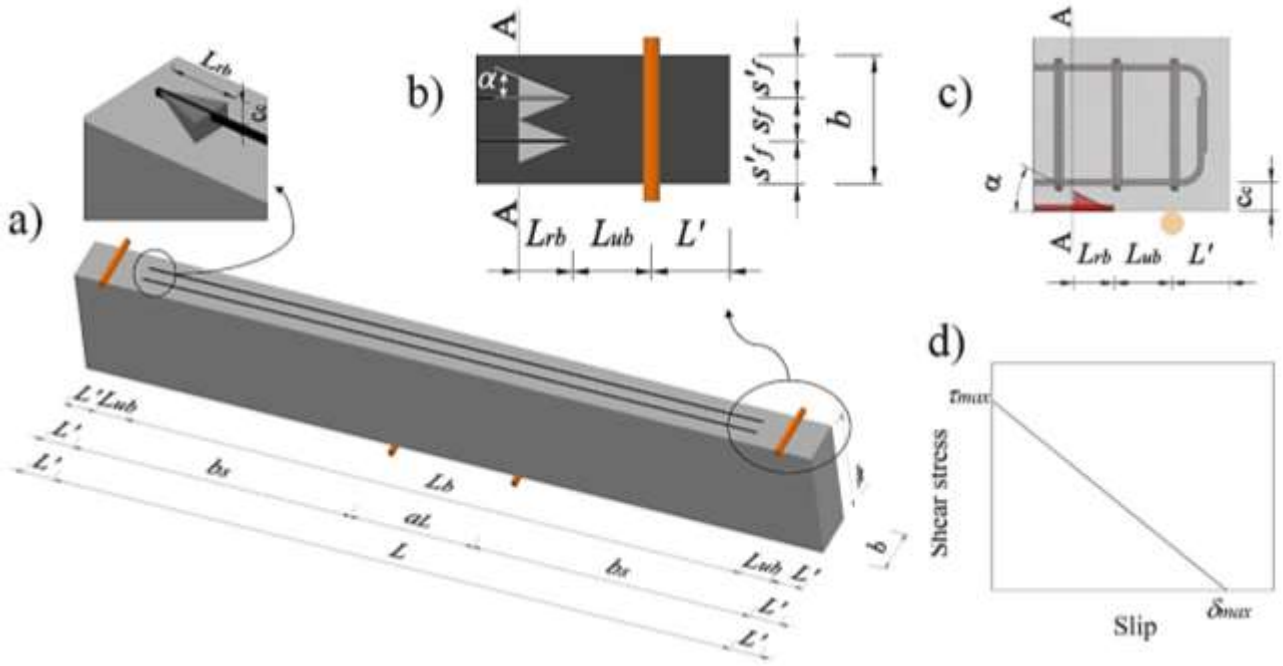


Figure 5: a) Characteristics of the bonded CFRP reinforcement, b) position of the CFRP laminates on the beam's tensile surface, c) concrete cover for the beam bottom face and resisting bond length, d) shear stress-slip relationship of local bond

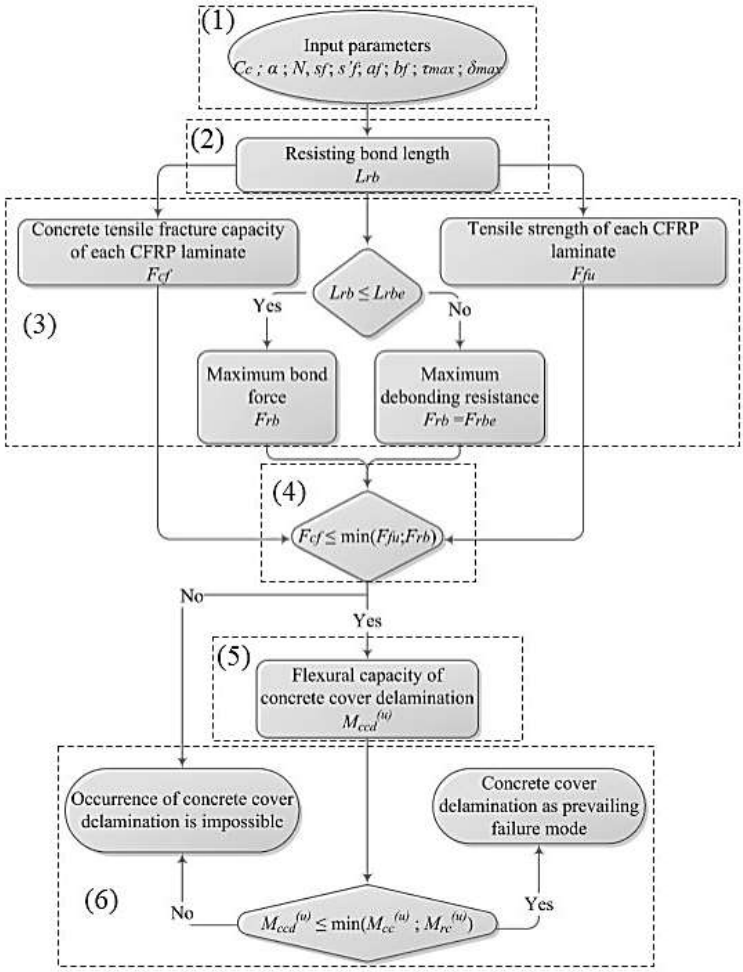


Figure 6: Calculation procedure for concrete cover delamination failure mode

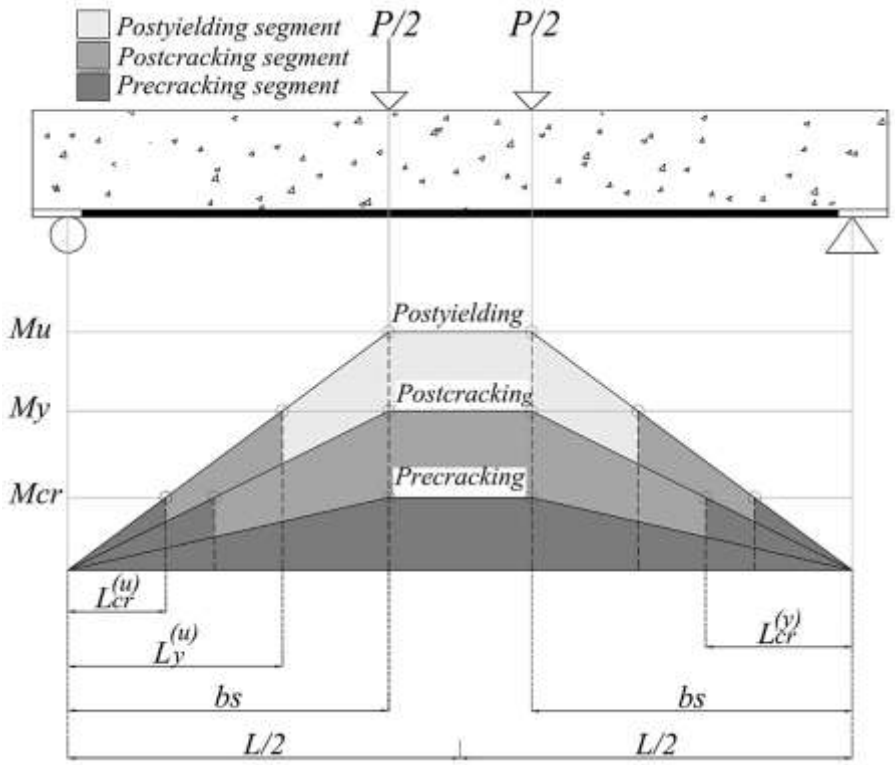


Figure 7: Distinct regions of the beam

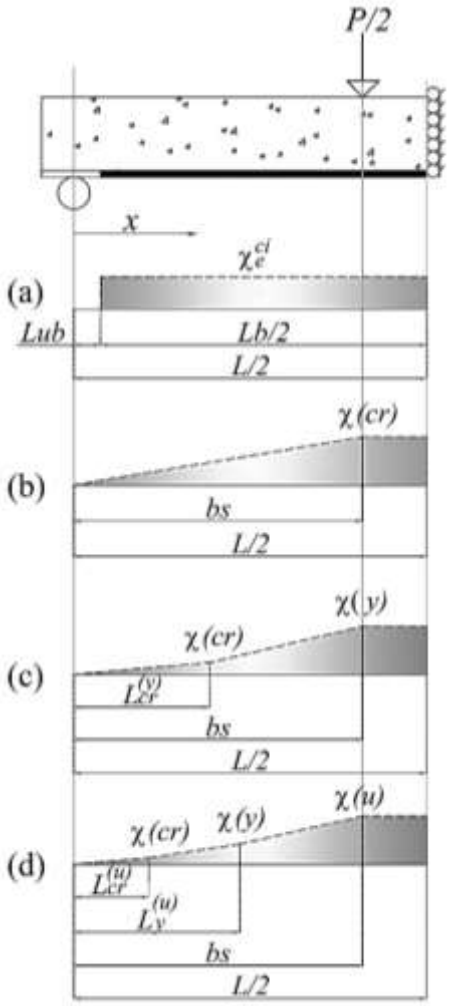


Figure 8: Curvature distribution along the beam length at the stages: a) initial camber, b) precracking, c) postcracking, d) postyielding

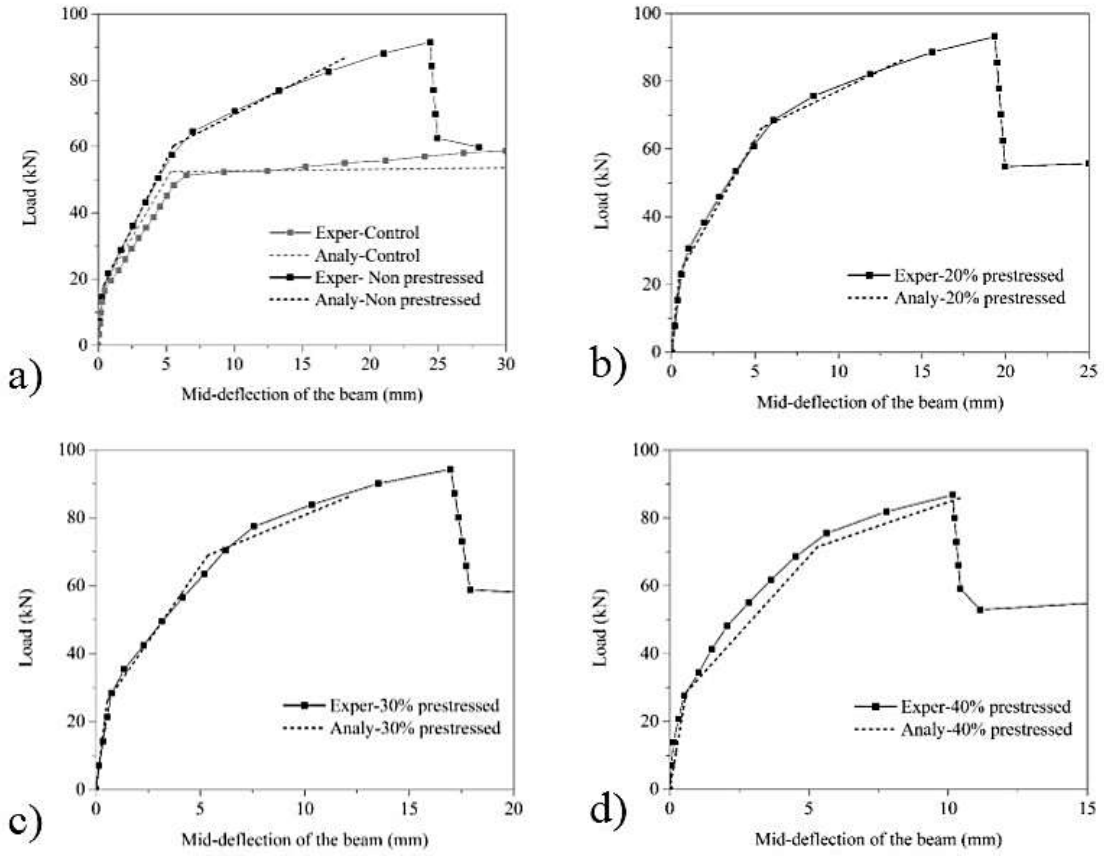


Figure 9: Analytical prediction of the tested beams of series 1 [13]: a) control and non-prestressed, b) 20% prestressed, c) 30% prestressed, d) 40% prestressed

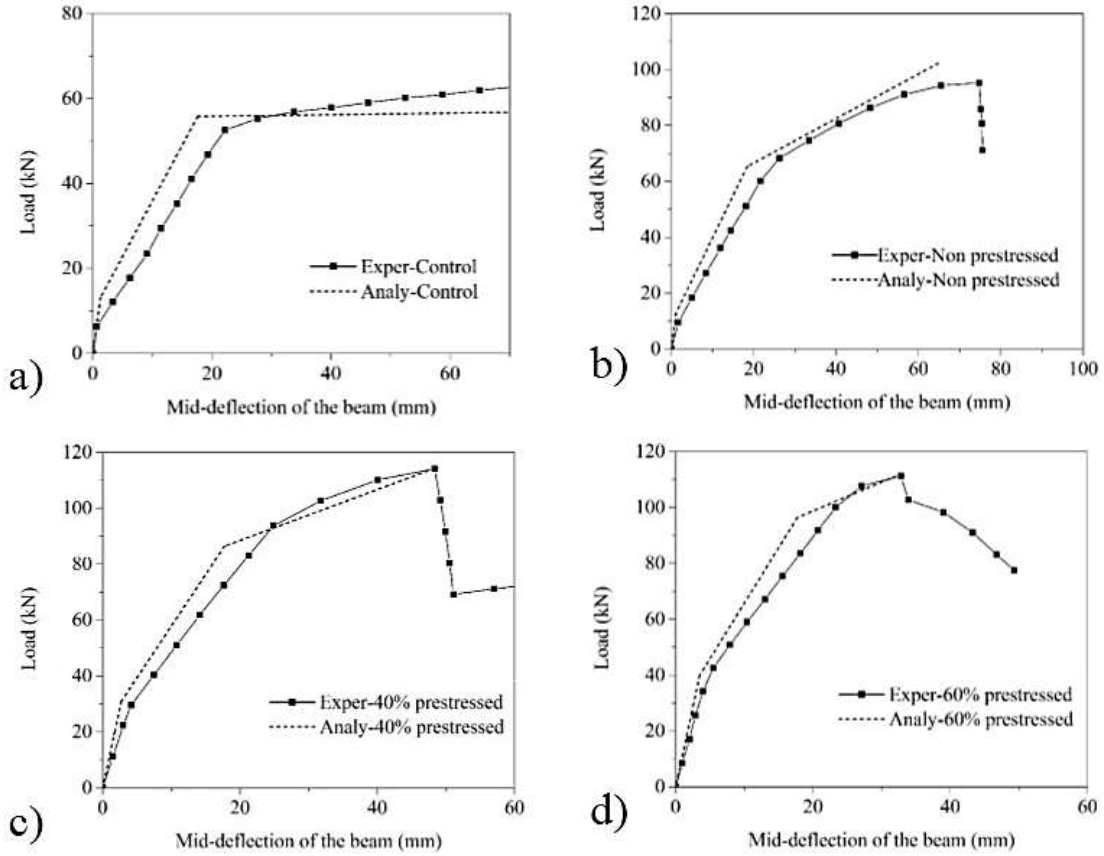


Figure 10: Analytical prediction of the tested beams of series 2 [11]: a) control, b) non-prestressed, c) 40% prestressed, d) 60% prestressed

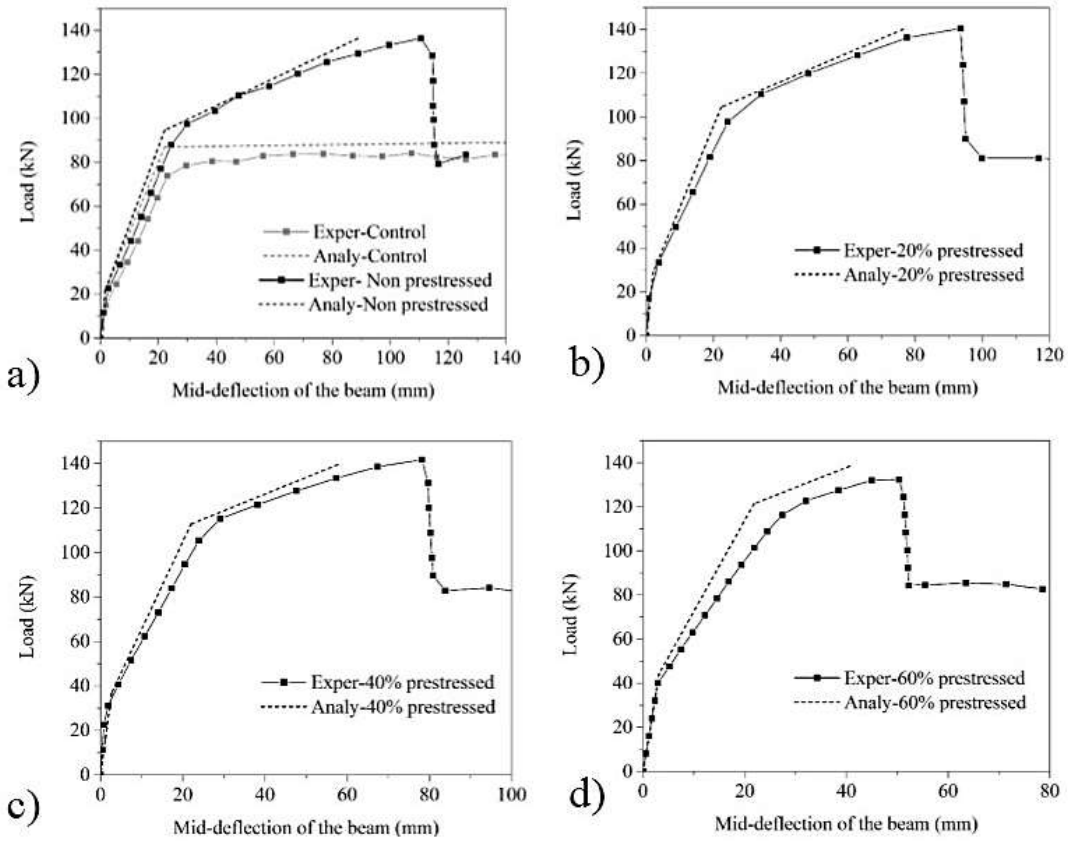


Figure 11: Analytical prediction of the tested beams of series 3 [12]: a) control and non-prestressed, b) 20% prestressed, c) 40% prestressed, d) 60% prestressed

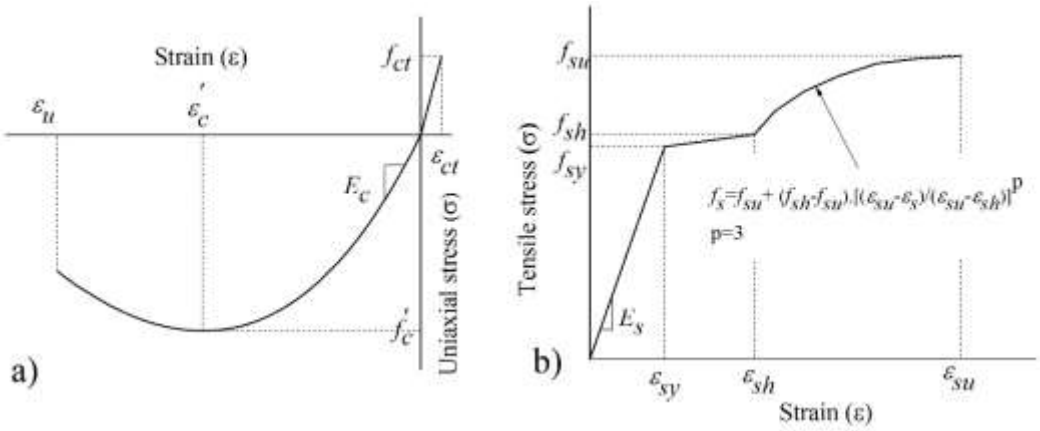


Figure 12: Stress-strain relationship used in DOCROS to simulate: a) concrete, b) steel bars

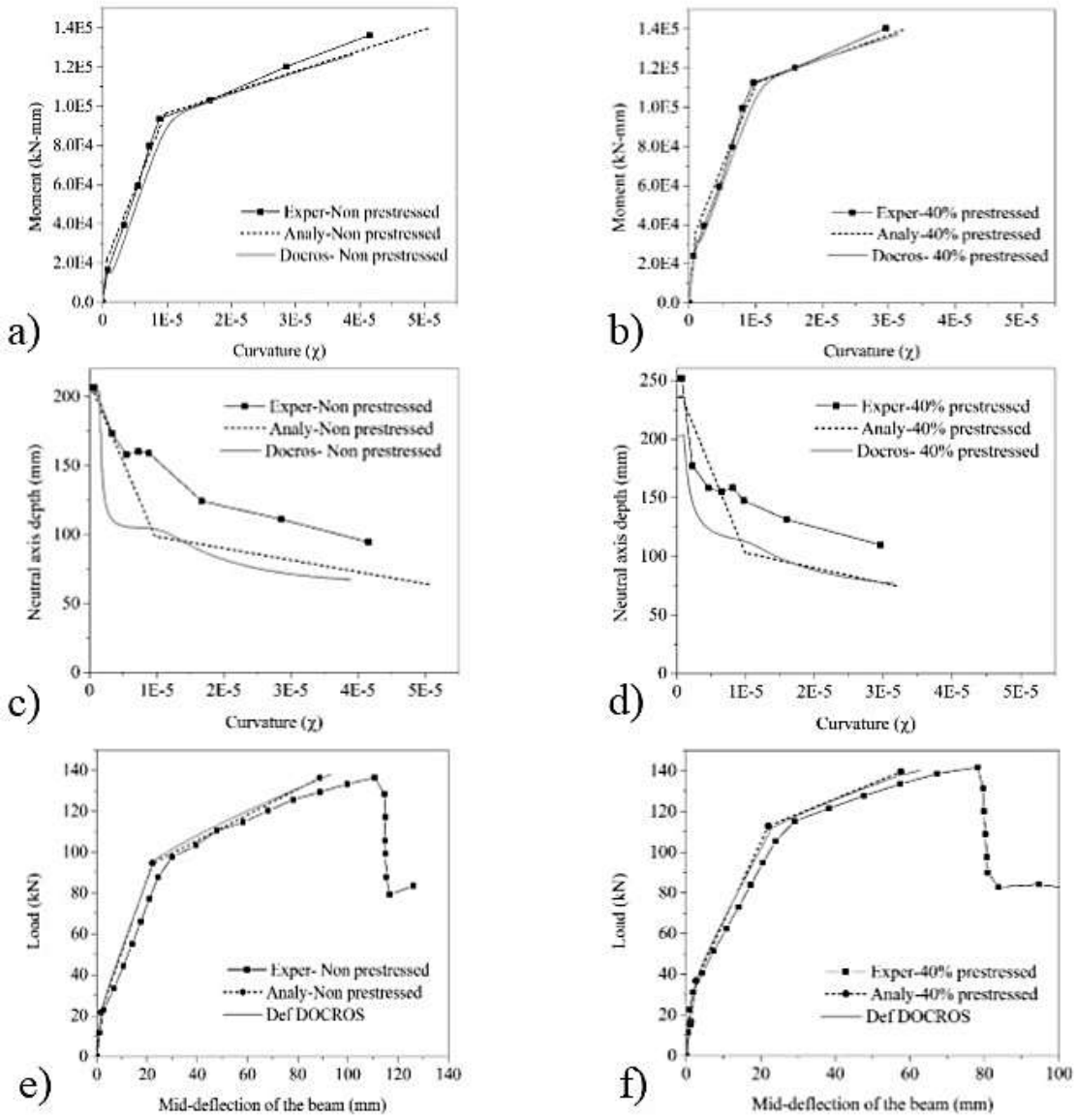


Figure 13: Experimental, analytical, and numerical (by DOCROS and Def-DOCROS) predictions of the beams in series 3 in terms of moment-curvature: a) non-prestressed, b) 40% prestressed, and neutral axis depth: c) non-prestressed, d) 40% prestressed, and mid-deflection e) non-prestressed, f) 40% prestressed

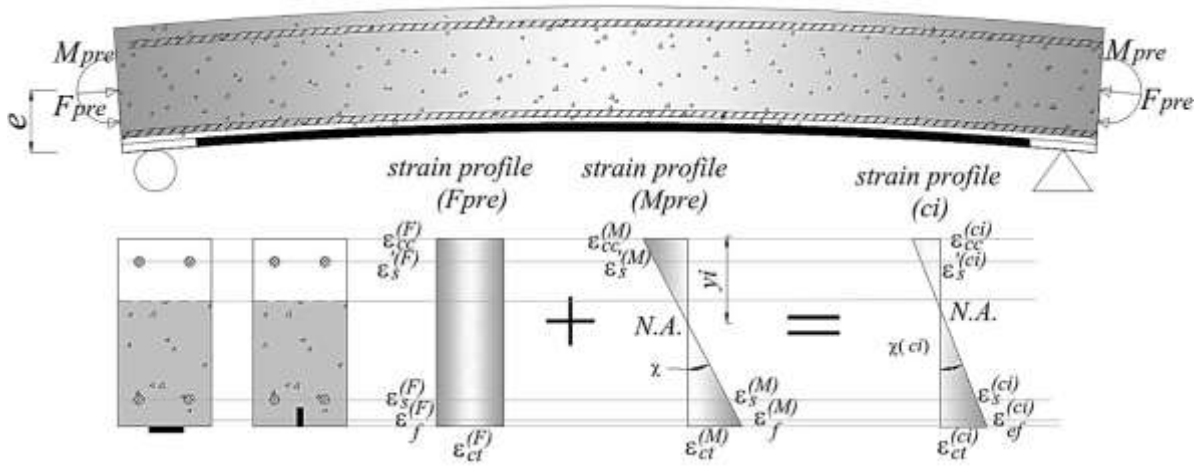


Figure 14: Strain profile of the prestressed section at initial curvature (ci)

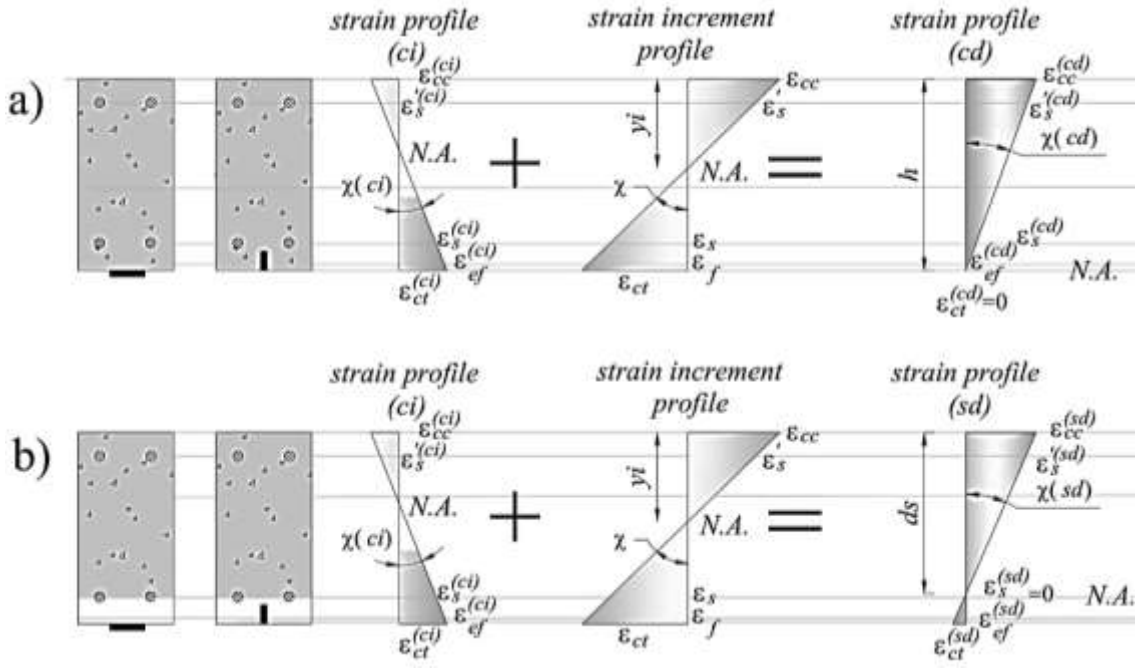


Figure 15: Strain profile of the cross section: a) at concrete decompression point (cd), b) at steel decompression point (sd)

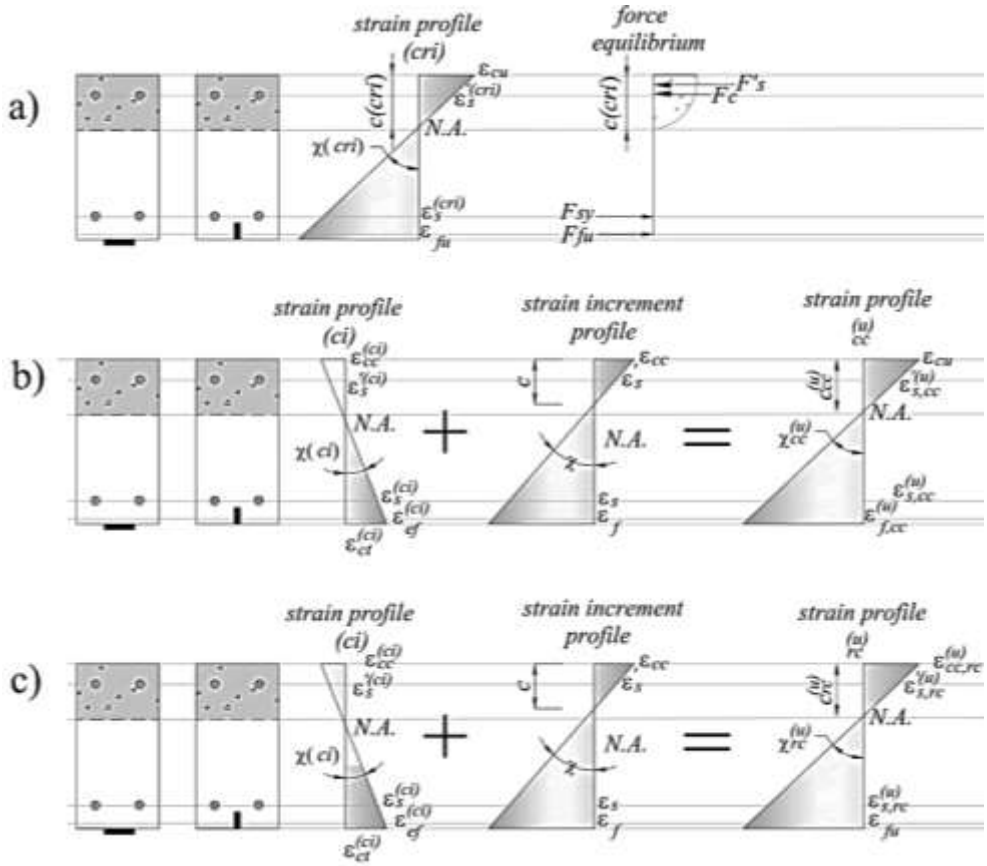


Figure 16: Strain profile of the cross section, a) simultaneous tension and compression failures (cri), b) compression failure (cc), c) tension failure (rc)